GROWTH HISTORY OF FAULT-RELATED FOLDS AND INTERACTION WITH SEABED CHANNELS IN THE TOE-THRUST REGION OF THE DEEP-WATER NIGER DELTA

**Byami A Jolly[1], Lidia Lonergan & Alex, C. Whittaker**

Department of Earth Science and Engineering, Imperial College London, South Kensington, London SW7 2AZ

Correspondence to Lidia Lonergan l.lonergan@imperial.ac.uk; +44 20 7596465

[1] now at Department of Geology, Ahmadu Bello University, Zaria, Nigeria (bjolly@abu.edu.ng)

**Accepted MARINE AND PETROLEUM GEOLOGY October-2015**

**Abstract**

The deep-water fold and thrust belt of the southern Niger Delta has prominent thrusts and folds oriented perpendicular to the regional slope that formed as a result of the thin-skinned gravitational collapse of the delta above overpressured shale. The thrust-related folds have grown in the last 12.8 Ma and many of the thrusts are still actively growing and influencing the pathways of modern seabed channels. We use 3D seismic reflection data to constrain and analyze the spatial and temporal variation in shortening of four thrusts and folds having seabed relief in a study area of 2600 $km^2$ size in 2200-3800 m water depth. Using these shortening measurements, we have quantified the variation in strain rates through time for both fault-propagation and detachment folds in the area, and we relate this to submarine channel response. The total amount of shortening on the individual structures investigated ranges from 1 to 4 km, giving a time-averaged maximum shortening rate of between 90 $\pm$10 and 350 $\pm$50 m/Myr (0.1 and 0.4 mm/yr). Fold shortening varies both spatially and temporally: The maximum interval shortening rate occurred between 9.5 Ma and 3.7 Ma, and has reduced significantly in the last 3.7 Ma. We suggest that the reduction in the Pliocene-Recent fold shortening rate is a response to the slow-down in extension observed in the up-dip extensional domain of the Niger Delta gravitational system in the same time interval. In the area dominated by the fault-propagation folds, the channels are able to cross the structures, but the detachment fold is a more significant barrier and has caused a channel to divert for 25 km parallel to the fold axis. The two sets of structures have positive bathymetric expressions, with an associated present day uphill slope of between 1.5$^{o}$ and 2$^{o}$. However, the shorter uphill slopes of the fault-propagation folds and increased sediment blanketing allow channels to cross these structures. Channels that develop coevally with structural growth and that cross structures, do so in positions of recent strain minima and at interval strain rates that are generally less than -0.02 $Ma^{-1}$ (-1 x $10^{-16}$ $s^{-1}$). However, the broad detachment fold has caused channel diversion at an even lower strain rate of c. -0.002 $Ma^{-1}$ (-7 x $10^{-17}$ $s^{-1}$).

**KEYWORDS**

Deep-water, Niger Delta, folds, thrusting, submarine channels, strain rate

## 1. Introduction

Passive margin, deep-water fold and thrust belts, such as that of the Niger Delta toe-thrust region, are areas of tectonic shortening in which the main driving force is the thin-skinned gravitational collapse of deltaic sediment wedges above a ductile substrate of weak shale (e.g. Niger Delta; Morley and Guerin, 1996; Cohen and McClay, 1996; Wu and Bally, 2000; Rowan et al., 2004; Billoti and Shaw, 2005) or mobile salt (e.g. Angolan passive margin, Gulf of Mexico; Cramez and Jackson, 2000; Anderson et al., 2000; Wu and Bally, 2000; Rowan et al., 2004). Contractional deformation within these fold and thrust belts is generally associated with the development of sedimentary growth sequences, deposited coevally with deformation. The growth sequences synchronously fill the accommodation space created by the growing structures and are characterized by stratal thinning or onlap onto the fold crests, and expansion away from the structural highs, into the associated piggy-back or mini-basins.

Submarine channel-levee systems are an important component of the deep-water depositional system (e.g. Normark; 1978, Walker, 1978; Deptuck et al., 2003; amongst many others) and consequently the pathways of sediment gravity flows are often influenced by the growth of structures at, or near the seabed. Folds and diapiric structures have been shown to divert, deflect, block or confine turbidite channels (e.g., Cronin, 1995; Huyghe et al. 2004; Gee & Gawthorpe 2006; Morley, 2009; Clark and Cartwright, 2009; 2011, 2012; Mayall et al., 2010; Oluboyo et al., 2014). Despite the growing number of studies addressing the interaction between active structures and submarine channels, there are very few studies that have attempted to examine in a more quantitative way the links between structural growth and submarine channel systems. The primary aims of this paper are (1) to quantify the spatial and temporal variations in syn-growth shortening of thrust structures and (2) for those with bathymetric relief assess how variations in these parameters have affected the pathways of submarine slope channels forming coevally with deformation.

The history of structural deformation can be determined by the geometries of the growth sequences associated with the growing structures. This means that, in principle, growth sequence geometries can serve as indicators of how variations in sedimentation and structural growth evolution have varied over time (e.g., Suppe et al., 1992; Burbank and Verges, 1994; Poblet and Hardy; 1995; Burbank et al., 1996 among others). The increasing availability of high quality 3D reflection seismic data driven by extensive hydrocarbon exploration in deep-water settings has led to a renewed focus on fold-related thrusting in deep-water gravitational systems (e.g., Corredor et al., 2005; Briggs et al. 2006; Higgins et al., 2007, 2009; Morley and Leong, 2008; Morley, 2009;

Maloney et al., 2010; Clark and Cartwright, 2012). The availability of such seismic data means that individual growth sequences can be mapped, and the shortening accumulated during the growth of folds and thrusts can be quantified. This information can therefore help to determine how strain varies through time in such settings, and how it may affect the sedimentary depositional systems that interact with the growing structures.

Because fold-related seabed bathymetry is likely to exert some control on the pathway of any sediment gravity flows an important issue is how shortening is related to the structural deformation of the seabed. It is conceptually simple to envisage how the growth of most types of fault-related fold should elevate the crest of the fold relative to its limbs, and relatively 'uplift' the seafloor. A number of attempts have been made to quantitatively understand the relationship between the structural elevation of the fold crest and the amount of fold shortening in fault-related folds using geometrical kinematic models (e.g., Suppe et al. 1992; Hardy and Poblet 1994; Poblet & Hardy 1995; Hardy & Poblet 1995; 2005; Poblet et al. 1997; Poblet et al., 2004). In general, uplift continues as shortening progresses except for the case of a simple fault-bend fold, where once the lowest unit in the hanging-wall reaches the upper footwall flat, the fold broadens (increases in width) without generating any further vertical relief. For other fold types, the conversion of shortening into a vertical component of uplift requires knowledge of an appropriate geometrical and kinematic model for the fault-fold type. Consequently in this study we clearly separate well-constrained estimates of fold shortening from estimates of crestal uplift.

Three-dimensional (3D) seismic reflection data from the toe-thrust area of the Niger Delta is used for our study. In this area, fold-thrust structures are well-preserved, and the deep-water setting minimises the problems of sub-aerial erosion that removes growth strata in terrestrial fold and thrust belts and tends to hamper similar studies on land. We mapped age-constrained stratigraphic horizons, in both the pre- and syn-kinematic strata, across actively growing thrust-related folds with seabed relief. We then used line-length balancing methods (Dahlstrom, 1969) to calculate the spatial (along-strike) and temporal variation in the cumulative strain that the horizons have accumulated in response to the continual growth of the folds. We discuss the implication of the strain variations at two scales; on a local scale to examine the effect on Pleistocene to modern seabed channel pathways through time, and at a large scale to elucidate the structural development of the Niger Delta.

## 2. Structural setting of the study area

The study area is in the eastern lobe of the outer fold and thrust belt of the deep water Niger Delta, at the down-dip contractional toe of the gravitational system, and covers an area of 75 km by 35 km (Fig. 1a). The Niger Delta forms the seaward-end of a NE – SW oriented failed rift basin called the Benue Trough. It formed during the opening of South Atlantic following the separation of Equatorial Africa from South America in Early Cretaceous times (Whiteman, 1982; Mascle et al., 1986; Fairhead and Binks, 1991). By Late Eocene times a delta had begun to build across the continental margin (Burke, 1972; Damuth, 1994). Today, the delta covers an area of 140,000 $km^2$ with includes both the subaerial fluvial delta and the associated deep-water slope to basin-floor depositional system. Stratigraphically, the delta has been divided traditionally into three diachronous units of Eocene to Recent age named the Akata, Agbada and Benin Formations (Short and Stauble, 1965; Avbovbo, 1978; Evamy et al, 1978; Whiteman, 1982; Knox and Omatsola, 1989; Doust and Omatsola, 1990). In the slope and deep-water parts of the Niger Delta, only the Agbada and Akata formations are recognised, where the Neogene mixed clastic slope and deep-water succession of the Agbada Formation overlies the pro-delta marine shales of the Akata Formation (Morgan 2004; Rouby et al., 2011). In distal deep-water regions the upper parts of the Agbada Formation consist of slope channel-complexes, mass-transport deposits and shales. Submarine channels flowing parallel to slope and perpendicular to structural trends have been identified and mapped at the seabed and in the shallow subsurface extending from the shelf edge to the deep-water Niger delta (e.g., Mitchum and Wach, 2002; Deptuck et al. 2003; Morgan 2004; Clark and Cartwright, 2012).

The delta is currently undergoing thin-skinned gravitational collapse (Damuth, 1994; Cohen and McClay, 1996; Morley and Guerin, 1996; Corredor et al. 2005) driven by differential loading of the advancing delta, resulting in downslope translation of the delta front and slope deposits on major detachment levels within the pro-delta marine shales of the Akata Formation (Bilotti and Shaw, 2005; Briggs et al 2006; Rouby et al. 2011). Three main structural zones are recognised within the Niger Delta: an extensional province onshore and beneath the shelf, with basinward dipping and counter-regional listric growth faults; a zone dominated by mud diapirism beneath the upper continental slope; and a down-dip, distal contractional zone (Damuth 1994) (e.g., Figs. 1a & 1b). Subsequently Corredor et al. (2005) further subdivided the deep-water contractional zone into two: an inner fold and thrust belt characterised by basinward-verging imbricate thrust faults and an outer fold and thrust belt characterised by both basinward- and landward-verging thrust faults and associated folds. The inner and outer belts are separated by a transitional zone with large, broad detachment folds interspersed with areas of little deformation (Fig. 1 a, b).

Previous studies of folding and thrusting in the deep-water Niger Delta have mostly focussed on the structural styles, evolution of the structures, and the structural controls on thrust and fold growth (e.g., Morley and Guerin, 1996; Bilotti & Shaw 2005; Corredor et al. 2005; Briggs et al. 2006; Higgins et al., 2009; Maloney et al., 2010). However, only a few studies have examined the structural control on the morphology of the submarine channels. At a broad scale Hooper et al. (2002) discuss how the structural evolution controls the development of accommodation space in the form of ponded-slope basins that are closely linked to the evolution of the associated thrusts. Degradation of emergent anticline crests was investigated by Heinio and Davies (2006) and the response of deep-water channels to growing structures has been documented by Morgan (2004) and Heinio and Davies (2007). Furthermore, a recent study in the deep-water fold belt of the western Niger Delta by Clark and Cartwright (2012) showed that a good understanding of the interaction between growth sequence architecture and growing folds can provide insight into the creation, and filing of accommodation space as folds grow through time. These authors also described the evolution of paleao-seafloor relief using growth sequences, and how the seafloor relief affected the primary sediment pathways through time.

Our study is located in the outer-most of the two fold and thrust belts (Fig. 1a), in water depths of 1700-2800 m below sea level where a number of folds with seabed relief can be seen to affect the pathways of modern submarine channels (Fig 2).

## 3. Dataset and Methods

### 3.1. Data and seismic interpretation

A time-migrated 3D seismic reflection dataset provided by Petroleum Geo-Services (PGS) was used for the study. It has a bin size of 50 m x 50 m giving a maximum horizontal resolution of 50 m. Based on the frequency content and assuming an average interval velocity of 2000 $ms^{-1}$, the data has a vertical resolution of approximately 13 m in the shallow Plio-Pleistocene section but decreases to ~30 m in the deepest parts of the section where seismic velocities are also expected to increase. The data are positive polarity, and are displayed with a black, positive, reflection indicating an increase in acoustic impedance.

The seabed seismic reflection was mapped throughout the 3D seismic volume and a seawater seismic velocity of 1490 $ms^{-1}$ was used to convert the two-way travel time seabed map to bathymetry (Fig. 2a). From the seabed bathymetry map, an edge-attribute map of the seabed and the seismic data, we identified modern seabed channels flowing down-slope from NE to SW and actively growing structures with seabed relief (Fig 2a,b). Seabed scarps and slumps are commonly associated with the fold crests (Fig 2b and 3). The four studied channels and folds are labelled in Figure 2. A tie-line provided by Shell across the two unreleased wells within the seismic survey area was used to constrain the stratigraphic ages for five seismic horizons between 23.2 Ma and 7.4 Ma, based on Shell's biostratigraphic data (*pers. com.* Shell Production and Development Company, Nigeria; 2011). A younger surface, which divides the main syn-growth unit into two packages, was also mapped. It was assigned an extrapolated age of 3.7 Ma by assuming a constant sedimentation rate in the main piggyback basin behind the major detachment fold, C, in the east of the study area. Periods of fold growth were constrained by mapping the syn-growth strata identified from onlapping reflector geometries, unconformities and thickness changes in the vicinity of the folds with thinning towards the fold crests and stratigraphic expansion into the inter-fold synclines (Figure 3). The onset of growth, as observed within the seismic data, occurs between the 12.8 and 9.5 Ma horizons (Fig. 3b). The 12.8 Ma horizon lies within the pre-growth strata, but the first evidence of thinning of strata on some fold flanks can be seen before the 9.5 Ma horizon, (see for example the backlimb of Fold D and backlimb of the next thrust to the south of fold D, Fig. 3). However, for the purpose of mapping we use the 9.5 Ma surface as a proxy for the base of the growth sequence although we recognise that in places, structures started to grow somewhat earlier. In this study we mapped seven seismic horizons, which include the 23.2, 15, and 12.8 Ma horizons within the pre-growth sequence, and the 9.5, 7.4, 3.7 Ma and seabed surfaces within the syn-growth sequences. The distribution, and thickness variations of the main growth package, from 9.5 Ma to the present day seabed, is illustrated in a two-way-travel time thickness map (Fig 4), and the strike of the four major structures studied are also labelled on this map.

### 3.2. Measurement of fold shortening

Shortening was measured by line-length balancing (Dahlstrom, 1969) on a series of dip sections spaced at approximately 2 km intervals along the fault-related folds of interest. The sections were pinned away from the structure at the point where the strata become horizontal, or pinned midway between two closely spaced structures. For pre-growth strata, a simple measure of shortening, $s_h$, can be defined as the summed length of the folded and faulted horizon measured between the section pin points (($L_o = P_1 + P_2$) in Figure 5), minus the present-day length, $\mathbf{L_f}$, between the same pin-points. However as the absolute value of shortening is dependent on the line-length chosen for the measurement, which may change along the length of the fold, where the fold changes in width for example, we considered strain (***e***) to be a more useful measure, where:

$$e = (L_f - L_o)/L_o \qquad \text{(Eq. 1)}$$

We note that the strain can easily be converted to a shortening factor, $\mathbf{S_f}$, where

$$S_f = L_f/L_o = 1 + e \qquad \text{(Eq. 2)}$$

hence a strain of -0.8 is the equivalent of a shortening factor of 0.2, or, in other words, the section has undergone 80% shortening. The syn-growth surfaces for which we measure strain are predominantly overlapping strata so, $L_o = S$ (Fig. 5). However, in cases where the syn-growth strata onlap the growing structure, a modification of methodology is required (see Poblet et al., 2004).

Erosion due to slumping is common on the front limb of the folds and forms significant scarps (Figs. 2b, 3b). For any syn-growth horizon truncated by a palaeo-scarp (such as horizon $h_3$ in Figure 6a) we measure the length by projecting the horizon across the scarp and over the structure while maintaining the overall shape of the structure (Fig. 6b). A similar approach was applied to the seabed for modern seabed scarps (Fig. 6c, 6d). Where recent-near recent channels have incised across a growing fold, we also extrapolated the stratigraphic horizon, over the growing structure(s), and into the channel fill as per horizon $h_3$ in Fig. 6(e, f). This method allows us to estimate the likely strain accumulated by the horizon assuming it had not been affected by slumping or channel incision.

Strain measurements were made for the seven seismic horizons mapped within the pre-growth and syn-growth strata on sections across the structures (e.g., section a2 across Fold A; Fig. 7a). From this the cumulative strain through time was measured– that is the cumulative summed difference in strain recorded between adjacent stratigraphic layers (Fig. 7b). The total shortening, or maximum cumulative shortening, recorded on the pre-growth strata occurs at the present day. If there has been no ductile thickening of the beds then the shortening calculated on any pre-growth surface should be constant for each pre-growth layer. From the cumulative strain it is simple to calculate an average interval strain rate between dated seismic horizons (Fig. 7c).

Shortening of folded and faulted layers has to be measured on sections where the horizontal and vertical scales are the same. This requires depth-converting the data; in the absence of velocity data we have assumed that the velocities in the depth range under consideration are likely to vary between 2100 $ms^{-1}$ (near seabed) and increasing to 2500 $ms^{-1}$ at depth and a mid-point velocity of 2300 $ms^{-1}$ was used. A test of the dependence of the results on changes on velocity is shown in

Figure 7 for Fold A. Increasing the velocity to 2500 m $s^{-1}$ changes the measurements by about 1–10 % at high values of shortening, and makes little difference to the cumulative shortening through time (Fig. 7b). The interval shortening rates are also similar regardless of seismic velocity used, although the percentage error is greater at smaller values of strain, normally within the younger syn-growth strata (Fig. 7c).

To view the variation in shortening along the length of each structure we plot the shortening for each surface against distance along the structure to produce a strain-distance diagram as is routinely done for extensional fault systems (i.e., displacement-distance plot). This was done using transects taken at approximately 1.5 km intervals along the strike of the structures. Similar diagrams have been constructed for displacement on active thrusts in New Zealand (Davis et al. 2005); and subsurface thrusts imaged on seismic data from the Niger Delta, Sichuan Basin in China, and the Magdalena Basin in Colombia (Higgins at al. 2009; Bergen and Shaw, 2010).

Limitations of the line-length balancing approach have been discussed in the literature in some detail (e.g., Hossack, 1979; Chapman and Williams, 1984; Moretti & Callot 2012). For example, any ductile thickening of the units during deformation where strain is accommodated by layer-parallel shortening will introduce errors. However our measurements typically show that strain for all horizons pre 15 Ma is approximately the same within measurement error which suggests that ductile thickening was not significant in the lower parts of the sedimentary units in the area, at least within the resolution of the data and our measurements. However Figure 7b suggests that some reduction in total strain is observed for the 12.8 Ma horizon in Fold A, which occurs before any significant growth strata are observed in the seismic data (Fig. 3b). There are two possible explanations; firstly there may be some ductile thickening of the 15-12.8 Ma interval, or secondly it may reflect some uncertainty in the location of the thrust fault (Fig 7a). The seismic signal is often degraded in the vicinity of the thrust faults towards the top of the pre-growth package which introduces uncertainty in the location of fault plane and hence position of horizon cut-offs (Fig. 7a). A single fault-plane was normally interpreted in such zones by positioning it mid-way through the zone of poor data quality, and the horizons were extended to intersect the fault plane, following the approach taken by Bergen and Shaw (2010). Error can also arise from the digitization of the horizon upon which strain is measured either by slightly increasing or decreasing the original length ($L_o$). Errors arising as a result of digitization are very small in absolute terms, and reach up to 0.5 % for higher strain values on the pre-kinematic units. However, they become relatively more significant when the absolute strain measurements themselves are very small, such as the younger syn-growth strata or older pre-growth strata with very low strain. In these cases the very low absolute strain values have error bars of comparable magnitude to the strain itself. Errors may also arise from the reconstruction of the seismic horizons that have been eroded on the fold crest (e.g., scarps and channel incision; Fig. 6). Unfortunately we have no information on the errors associated with the stratigraphic ages and therefore cannot assess any potential effect on the calculated interval strain rates. The majority of these limitations will affect the absolute value of shortening derived, but as this paper focuses on the relative variation in shortening both through time, and along the strike length of the structures, it is considered that the approach used is robust enough for the purpose of the study.

## 4. Results and observations

### 4.1. Structures and fold geometries

The western half of the area is dominated by closely-spaced, fault-propagation folds with a linear NW-SE trend (Figs. 2b, 3, 4). Many fold crests are separated by only 2 – 3 km. In the east, a 10 km wide, arcuate, fold (Fold C) dominates; it forms the southern boundary to a synclinal, piggyback basin which is at least 20 km wide (Fig. 4). Generally the synclinal basins located between folds and thrusts contain up to 2000 ms TWTt of syn-growth strata with significant thinning onto the crests of the structures (Figs. 3, 4). The thrust faults of the fault-propagation fold structures terminate within the lower parts of the syn-growth strata, and rarely intersect the 3.7 Ma horizon, with no faults extending to the seabed (Fig. 3). Many of the structures in the area are buried (Figs. 3, 4). We focus on four folds (A – D; Figs. 2 and 4) which can be traced for up to 35 km along strike, have seabed expression and deform the seabed, and hence demonstrate evidence for on-going growth. Although the folds have a relatively simple expression at the seabed, with associated seabed scarps where the structural relief is highest (Figs. 2b, 3b), some are more complex structures at depth.

Fold A extends outside the study dataset. It is linear in plan view and formed above a seaward-verging forethrust dipping at c. 28 – 31° which detaches within the Akata shales (Fig. 8). An antithetic backthrust, which intersects the main thrust, deforms the back limb of the fold. The faults die out upwards within the folded syn-growth strata and deform, but do not offset the 3.7 Ma horizon. Seabed scarps, up to 250 m in height, occur along the fold in regions of higher structural relief (e.g., Fig. 2b; Fig. 8 a,b). Fold A is interpreted to be a fault propagation fold forming in response to on-going shortening in the toe region of the Niger Delta.

Fold B is a composite structure consisting of two, closely spaced thrusts. Along the north-western half of the mapped fold trace (solid line Figs. 2, 4) the seaward thrust dominates the structure and has the highest structural relief (Fig 9b). Seabed scarps form on the frontal side of the associated fold. A second thrust cuts the backlimb of the frontal thrust and is buried at the present day but was active until at least 3.7 Ma. In contrast, on the south-eastern half of Fold B, the more landward of the two thrusts takes over as the dominant structure, with highest structural relief (Fig. 9d) and the frontal thrust is buried (dashed line on Figs. 2a, 4). Because the two thrusts are so closely spaced, for the purposes of calculating the shortening it is necessary to calculate the strain across both structures to allow a consistent pin-point for the line-length measurements on both flanks of the overall fold.

Fold D is also a composite structure, where the more landward of the two folds is the one with seabed expression, while the frontal fold has been buried since at least 3.7 Ma (Fig. 9 e,f). In contrast to Fold B, the relationship between the two structures remains consistent along the fold length (Fig. 2a). Again, to get consistent shortening estimates the two structures are considered together. In the same way as Folds A and B, fold D also has well-developed seabed scarps, with a seabed relief of up to 280 m (Fig. 2b).

In contrast, Fold C, in the east of the area (Figs. 2a, 4), has a very different geometry. It is a much broader, longer wavelength anticline (>5 km), with low displacement planar thrusts on the front and back limbs, and in places in the fold core (Fig. 10). A key difference between Fold C and the other folds is the thickening of the Akata shale observed under the fold crest. Some of the thickening is due to imbrication within parts of the Akata shale itself (Fig. 10). In the core of this fold, the top of the Akata shale is approximately 800 ms (TWTT) shallower than in the fault-related folds in the west of the area. The first-order geometry of this anticline is similar to a detachment fold where the folding is driven by thickening at the detachment level (Jamison, 1987). Fold C may be the along strike continuation of a similar structure documented by Maloney et al. (2010), from an area just to the east of our study.

**4.2. Channels and interaction with structures**

The four Pleistocene to Recent channels that are the focus of the study can be identified clearly on the seabed bathymetry and edge map together with a buried channel (Figs. 2b; 11b). Regional seabed bathymetry maps compiled from 3D seismic datasets shows that these channels largely originate from the shelf edge region of the Niger Delta (*pers. com*. PGS, 2013; Mitchum and Wach, 2002). The channels are mostly erosionally confined, but are also partially associated with constructional levees (Fig 11 a, b). They all have a well-defined erosional base, (e.g. cyan surface on Fig 11b), with a complex internal fill made up of a number of smaller cut and fill channels. The lowermost erosional surface that defines the base of the channel complex defines a channel system that can be up to 4 km wide and contains a maximum total fill thickness of between 100-350 m. The seabed expression of the channels is defined by the youngest, most recent erosional surface (Fig 11, a, b). The channel complex fills are characterized by medium to high amplitude, discontinuous, chaotic seismic reflections, with several erosion surfaces within the main channel complexes. The levees, where present, are up to 4 km in lateral extent and are characterised by low to high amplitude, continuous seismic reflections that thin laterally away from the main channel axis, defining a wedge-shaped geometry (Fig 11b). Most of the Pleistocene – Recent channel levees appear to downlap onto a seismic surface that is estimated to be approximately 1.2 – 1.3 Ma (Fig. 11) which implies that the channels are approximately of that age and younger. While it is difficult to accurately determine the relative ages of the individual, our interpretation suggests that channel 4 is the oldest, followed by channel 3 and that channels 1 and 2 are the youngest.

The channels display a range of interactions with the active structures (Fig 11c) which include deflection around fold tips (e.g., channel 4); diversion parallel to a structure (e.g., channel 2) and incision across the centre of growing structures (e.g., channel 1). Channels 1, 3 and 4 are transverse to structure and predominantly run in a NW-SE direction parallel to the slope gradient except where they interact with active structures (Figs 2a, 11c). Channel 4 is deflected at the lateral tips of Folds D and B. It is then diverted to a more southerly path as it approaches Fold A, before cutting through Fold A where it then joins, or is captured by Channel 1. Channel 1, in contrast cuts through Fold B, but Channel 3, is deflected slightly to the south prior to joining Channel 1 where Channel 1 cuts across the fold. Channel 2 exhibits a somewhat different behaviour. It flows down through the piggyback basin behind fold C and it is diverted by approximately 25 km in a SW direction to end up running almost perpendicular to the regional seabed slope behind Fold C. Beyond the tip of Fold C it too joins channel 1.

**4.3. Temporal and spatial variation in fold shortening**

The calculated shortening through time, expressed as strain, is shown for four representative sections, a1, b1, c2, and d1 across each fold (Fig. 12a). The total (maximum) shortening is the strain recorded on the pre-growth strata at the present day and hence is the intercept on the y-axis in the cumulative strain graph. The sections chosen for this calculation are at strain maxima. Folds D and B, which each include two fault-related, fold structures (*cf*. Fig. 9) have shortened by 3810 m and 3430 m respectively. This equates to a strain of -0.35 and -0.32. The shortening of Fold A is lower (1470 m) with a strain of -0.15. Fold C has only shortened by 1027 m and so has a significantly lower strain than the other structures (-0.06 ; Fig 12a). The shortening started between 12.5 and 9.5 Ma for all structures investigated (Fig. 12a). The three fault propagation folds, A, B and D respectively, then grew at a faster rate between 9.5 and 3.7 Ma. In contrast, the detachment fold (Fold C) grew at a low, almost constant rate until 7.4 Ma when it then showed a modest increase in rate until 3.7 Ma. In the last 3.7 Ma growth on all the structures has slowed (Fig. 12a). Folds A, B and D record the highest, average interval strain rates, with values of 0.02 and -0.06 Ma$^{-1}$ (or -1E-16 and -15 s$^{-1}$), from 9.5 to 3.7 Ma (Fig. 12b). For Fold C, the strain rate values are very low (< -0.01 Ma$^{-1}$), although there was a small increase in rate to almost 0.01 Ma$^{-1}$ between 7.4 and 3.7 Ma (Fig. 12b).

The larger maximum strains recorded for Folds B and D are not surprising because in comparison to Fold A, Folds B and D are composite folds formed by two fault-propagation faults. The results are interesting in that if we assume equal contribution of both structures in B and D to the total strain, to a first approximation individual fault-propagation fold structures in this part of the Niger Delta have almost the same maximum cumulative strain. It also appears that the strain accumulated at very relatively similar rates (-0.02 to – 0.06 Ma$^{-1}$), at least within the temporal resolution of our data.

The pattern of strain distribution along the strike of the folds is shown in Figure 13 for a single pre-kinematic horizon (23.2 Ma) and three other syn-kinematic horizons, 7.4 Ma, 3.7 Ma and the seabed respectively. For Folds B and D the strain reduces towards the fold tips, while for Folds A and C, the folds continue outside of the survey area, so the lateral tips are not observed. Folds B and D have broadly 'bell'-shaped shortening profiles, which is characteristic of structures that grow by lateral propagation. Strain is highest on the oldest pre-kinematic horizons and declines over time, consistent with the data in Figure 12. For all three of the folds, local minima are seen between regions of higher strain. Such local minima in both thrust and normal fault systems are typically interpreted as the signature of segment linkage (e.g., Davis et al. 2005; Higgins et al., 2009; Bergen and Shaw, 2010, for thrust systems and Cartwright et al., 1995; Gawthorpe and Leeder, 2000 amongst many others for normal faults). Significantly, the minimum in the strain profile for the composite Fold B at 18 km strike distance coincides with the position where the switch occurs in dominance of the two thrusts that make up Fold B (Fig. 2a). So although neither fault-propagation fold tips out at this position, the cumulative shortening is at a minimum at this position at all times during the formation of the fold, including at the present day. However, in detail the along-strike, strain-distribution maxima and minima are not always in the same location for each stratigraphic horizon. At the 10 km position on Fold A for example, maxima or relative highs in the 23.2 and 7.4 Ma horizons actually correlate with strain minima at the 3.7 Ma and seabed surfaces. At a position of 15 km along this fold the opposite occurs, and again at 30 km a broad minimum in the older two horizons corresponds with a high in the 3.7 Ma surface. In Fold C, the strain variations in along strike distance also show possible fold segments identified in the older horizons, but the youngest syn-growth strata (seabed) does not show the same number of segments. This may suggest early linkage between fold segments and once linked, younger growth strata record shortening of a single structure, and that linkage points do not necessarily remain the location of persistent low displacement. For the detachment fold C, the accumulated strain is low compared to the other structures (Fig. 12). The maximum strain recorded by this structure is less than -0.06, which is approximately one third of the maximum strain recorded for Fold A, which is also a single structure and not a composite structure as are Folds B and D.

### 4.4. Strain variation and submarine channel response

Using the temporal and spatial evolution of strain through time, we can evaluate how the shortening in the toe-region of the Niger Delta affected pathways of submarine channels in the area. In the north of the study area, channel 4 is deflected around the tip of Fold D, where there is a minimum in the present day bathymetric expression of the fold (Fig 11c). When the position of Channel 4 is plotted on the strain-distance graph, the channel has been deflected to the region of lowest cumulative strain at the tip of the fold (Fig. 14, D1). In addition, if the interval strain rates for two positions along the fold are examined- firstly at position [1], towards the centre of the fold, and secondly at position [2] towards the fold tip, the rates at position [2] are consistently lower than those at position [1], for the entire growth period of the structure, and the strain rate was at its lowest value (approximately -0.0023 $Ma^{-1}$ or $-7 \times 10^{-17}$ $s^{-1}$) during the last 3.7 million years (Fig. 14, D3). These data indicate that channel 4 is exploiting this region to cross Fold D because it has been a region of low bathymetric relief, due to being a local strain minimum throughout the lifetime of the channel.

However, down-system to the south, both Channel 4 and Channel 1 cross Fold A in an area where the total cumulative strain since the Miocene is high (ca. -0.15), and close to a maximum for this structure (Fig. 14, A1 and A2). Although this position is one of high *total* strain for the structure, it is a point of *low* strain rate for the 3.7 Ma to recent interval with a rate of -0.0016 $Ma^{-1}$ ($-5 \times 10^{-17}$ $s^{-1}$; Fig. 14, A1, A3). Channel 4 was deflected southward as it approached the fold to cross the fold at a position of strain minima in the 3.7 Ma horizon, instead of continuing down slope and crossing the fold at a position of relative strain maximum (at distance positions 29-30 km in Fig 14, A1 along the fold strike).

Fold B, in the center of the study area, is incised by Channels 4, 3 and 1. The seabed map shows that Channel 4 is deflected to the fold tip, crossing in a region characterized by low cumulative strain values on the older stratigraphic horizons, and also low strain for the younger stratigraphic horizons, where the interval strain rate from 3.7 Ma to present is -0.0026 $Ma^{-1}$ (-8.4 x $10^{-17}$ $s^{-1}$) (Fig. 14, B1 and B2). Similarly, Channels 1 and 3 also cross close to the local strain minimum on Fold B where displacement is transferred between the two structures that form the composite fold (Fig. 14, B2). Channel 3 deflects from its original course to join with Channel 1 upstream of the position where both channels cross the active structure. However, despite being a local strain minimum, the cumulative strain of the older 23.2 and 7.4 Ma horizons is still relatively high at this position at -0.16 and -0.28 respectively, but importantly the cumulative strain for the interval in which the channels were active (3.7 Ma to Recent) is very low. Likewise the interval strain rate is very low for this interval (approximately -0.0022 $Ma^{-1}$ or-7.2 x $10^{-17}$ $s^{-1}$) and is similar to the values calculated for the same interval where Channel 4 crosses Fold D and Channels 1 and 4 cross Fold A.

In comparison, Fold C has a much lower cumulative strain over its entire history than the other three folds examined (Fig. 14, C1). The maximum cumulative strain is about 15 % that of Folds D and B and 30 % that of Fold A. The interval strain rate for the time of channel development is consequently also very low, reaching only -0.0023 $Ma^{-1}$ (-7.3 x $10^{-17}$ $s^{-1}$; Fig. 14, C3). Nevertheless, this structure is still able to cause the diversion of Channel 2 for up to 25 km before the channel finally deflects around the fold tip and joins with the other channel systems (Fig. 14, C2, Fig. 2a).

In summary, the seabed channels in this part of the Niger Delta can keep pace with the growth of fault-propagation folds whose interval strain rates are between -0.002 to -0.0022 $Ma^{-1}$ (-5 and -7.2 x $10^{-17}$ $s^{-1}$) for the time period from 3.7 – 0 Ma. For the broad, detachment fold with a longer wavelength of uplift field, even lower maximum strain rates -0.0023 $Ma^{-1}$ (-7.3 x $10^{-17}$ $s^{-1}$) caused a seabed channel to be diverted.

## 5. Discussion

Our results show that the spatial and temporal variation in shortening along major thrusts and folds having seabed relief has played an important role in controlling the position of submarine channels in the Niger Delta. We now address how the relative rates of fold growth and apparent sediment accumulation help to constrain when structures have positive bathymetric relief on the sea bed, and we consider how shortening might be converted into estimates of the vertical uplift rates with which submarine channels are able to keep pace. Finally, we discuss the implication of the strain results for the structural evolution of the Niger Delta gravity driven system.

### 5.1. Fold growth and sediment accumulation rate

Where fold growth is associated with the deposition of syn-growth units, two conceptual end-member models can be used to describe the relationship between sediment accumulation rate and structural uplift rate (Fig. 15). The ratio of the amount of sediment accumulation to the rate of structural uplift determines whether a structure develops a bathymetric expression on the seafloor (Burbank and Vergés, 1994, Burbank et al., 1996, Ford et al., 1997, Broucke et al., 2004, Shaw et al., 2004, Shaw et al., 2005). For example, when the sediment accumulation rate is greater than the uplift rate of the structure, the deposited sediments will thin over the crest of the structure, forming overlapping stratal geometries and there will be smooth or flat seabed bathymetry (Fig. 15a). Seabed channels would be expected to cut across the structure as shown Figure 15b, and will not be deflected by it because there is no associated positive bathymetric relief. However, when the structural uplift rate is greater than the sediment accumulation rate (Fig. 15c), the syn-growth sediments will onlap the structure and a bathymetric expression of the growing structure will remain at the seabed. Consequently, seabed channels would be expected to divert to the lateral tips of the structure as a result of the development of positive bathymetric relief (Fig. 15d).

In reality the stratal geometries observed on the flanks of structures are not often this well-defined, and both onlapping and overlapping geometries can occur on the same fold, as either sediment supply or growth rates vary through time (e.g. Shaw et al. 2004). In our study for example, two groups of structures were identified – the fault-propagation folds that largely occur in the central and western parts of the study area (folds A, B, D), and the broad detachment fold (C) that occurs in the eastern part of the study area. Since 3.7 Ma, within resolution of the seismic data, the syn-growth sediments in the fault-propagation folds largely overlap the crest of the growing structures as shown in sections across Folds A and D in Figure 16 (a, b). However they are still associated with a tilt of the present day seabed and there is a 2 km landward-facing uphill slope on both of these folds (Fig. 16a, b) of between 1.5$^{o}$ and 2$^{o}$ on the up-dip, north-easterly dipping limb of the respective anticline. The presence of this uphill slope, coupled with the overall thinning of the growth sequences at the structural culmination of the fault-propagation folds, does suggest the presence of a slight positive bathymetric relief for most of the recent growth history albeit having an overall marginally greater sediment accumulation rate relative to structural growth rate. Consequently, the fault-propagation folds in the central parts of our study area lie somewhere close to the end-member model (a) in Figure 15.

On the other hand, the detachment fold in the east of the study area, lies closer to end-member model (c) in Figure 15 because the syn-growth sequences associated with this structure since 3.7 Ma, largely onlap the fold (Fig. 16c). On close examination, these syn-growth units show periods of minor offlap (continuous yellow lines, Fig. 16c) within overall onlapping geometry. These discrete, alternating packages of onlap and offlap within overall onlapping geometry, suggest variations in either the growth rate of Fold C through time, or the rate of sediment accumulation in the area. Fold C also has a similar uphill slope of between 1.5$^{o}$ and 2$^{o}$, on its northerly dipping limb, but it has a longer wavelength uphill slope of up to 5 km when compared to the fault-propagation folds (Fig. 16c). In addition to the difference in uphill slope length, the fault-propagation folds are only 2 to 3 km wide whereas Fold C is characteristically very broad (up to 10 km wide, *cf.* Fig. 4).

### 5.2. Shortening versus vertical uplift

An important issue is the conversion of horizontal fold shortening and strain rate to the vertical component of growth. In general, all cases of fault-related-folding will generate vertical uplift associated with shortening. This uplift continues as shortening progresses except for the case of a simple fault bend fold, where once the lowest unit in hanging-wall reaches the upper footwall flat, the fold broadens (increases in width) without generating any further vertical relief. Conversion of shortening into a vertical component of uplift requires an appropriate geometrical and kinematic model for the fault-fold type under consideration (e.g. Hardy and Poblet, 1994; Poblet and Hardy, 1995), which means that estimates of uplift are tied to the model chosen. For fault-propagation folds there are a number of kinematic models and the precise final shape of the fold depends on whether flexural slip (e.g., Suppe and Medwedeff, 1990) or a trishear model (e.g., Allmendinger, 1998) is assumed. Within the flexural-slip suite of models, two cases often considered are that of a constant limb thickness, or a fixed axial surface that allows for thickening or thinning in the frontal limb of the fold (Suppe and Medwedeff, 1990; Hardy and Poblet, 2005). For these geometries both models predict an almost linear relationship between uplift and shortening (e.g., Storti and Poblet, 1997). Hardy and Poblet (2005) also investigated the relationship between uplift rate, fault geometry and slip rate using a velocity description of deformation for both fault-propagation and trishear folds. Their results show that the velocity field varies in the back-limb, crest and forelimb of the structure. When they compare velocity models of a trishear fold versus a fault-propagation fold, they show that the uplift rate above trishear fold crests is smaller than for fault-propagation fold models. One method proposed by Bernard et al. (2007) and subsequently applied to emergent growing folds in the Tienshan, Taiwan and the Chinese Pamir (Daeron et al. 2007; Simoes et al. 2007; Li et al. 2013) uses another analytical, velocity-based model, derived from an analogue sandbox model of a growing fault-tip fold to relate fault slip to vertical rock uplift. This model likewise shows that uplift rate can vary within domains with separate axial surfaces defined for the fault-related fold.

For our purposes, we are interested in approximating the vertical uplift magnitude produced by the growing folds in the last 3.7 Myr over which the channel systems have been active. While the kinematic approach does have its limitations, we choose to estimate the vertical uplift in the crestal area using the methodology of Hardy and Poblet (2005) for fault propagation folds, a geometry which is appropriate for folds A, B and D. Making the reasonable assumption that the decollement surface the fault detaches into is approximately horizontal, we can use the model of a single step flexural-slip fault propagation fold to estimate crestal uplift. In this case the uplift rate, *u*, at the fold crest is given by

$$u = 2\,\dot{s}\,\mathrm{Sin}\ \theta \qquad \text{(Eq. 3)}$$

where $\dot{s}$ = slip rate, and $\theta$ is the fault dip (obtained here from a depth conversion of the seismic data and estimated to be between 28 and 31 degrees). Alternative fault propagation fold geometries considered by Hardy and Poblet (2005) produce results which differ in detail but are similar in order of magnitude terms (e.g. a trishear model produces exactly half the crestal uplift of the equivalent single step flexural slip fault propagation fold), so we consider this approach robust enough for our purposes.

Clearly use of Eq. 3 requires the conversion of our fold shortening ($s_h$) estimates to a slip rate, which we do using the relationship:

$$= \frac{s_h}{\mathrm{t}\cos\theta} \qquad \text{(Eq. 4)}$$

where *t* is the time frame of reference. Resultant uplift rates (m/Myr) for the fault-propagation folds (A, B and D) over a period of 3.7 million years are shown in Table 1. The maximum shortening measured across Folds A, B, and D in this study, is -216 m, -198 m, and - 204 m respectively. Using a fault dip angle of *ca.* 30°, these translate to an approximate crestal uplift of 218 m, 202 m, and 216 m respectively over this time period. Estimated uplift rates are therefore 59 m $Ma^{-1}$, 54 m $Ma^{-1}$, and 58 m $Ma^{-1}$ respectively, equivalent to 0.05 - 0.06 mm/yr (Table 1). Overall, these calculated values of crestal uplift rate are similar in magnitude to the shortening documented on the folds from 3.7 Ma onwards.

Fold C has a lower documented cumulative shortening (169 m), but as it is a detachment fold, rather than a fault propagation fold, the method outlined above is likely to be inappropriate for this structure. For detachment folds there are a wide variety of model outputs for uplift that depend on the geometric assumptions made. In the Dahlstrom (1990) model, where fold limbs lengthen as dip increases and folds grow, the relationship between uplift and slip is linear (Poblet and Hardy, 1995). In contrast, for the classic De Sitter (1956) model for detachment fold growth, where the fold grows by an increase in limb dip, or progressive limb rotation, then the relationship between uplift and slip is highly non-linear, with significant uplift accrued at low slip values, with the rate of additional uplift generation decreasing markedly as cumulative slip increases (e.g., Hardy and Poblet, 1994; Poblet and Hardy, 1995; Storti and Poblet, 1997). Distinguishing between these possibilities is not easy for Fold C so we do not estimate an uplift rate although this is likely to be less than for the fault propagation folds. Nevertheless, the growth of this broad fold has led to the diversion of channel 2, while channels 1 to 3 have been able to incise across Folds A, B and D which are growing at ≥ 0.05 mm/yr.

### 5.3. Channel response to active deformation

Our analyses show that all structures affecting channel pathways are associated with some bathymetric relief, but the length of the landward-facing uphill slope varies (approximately 2 km for the fault-propagation folds and up to 5 km for the detachment fold). Whilst the syn-growth sediments largely overlap the fault-propagation folds, the presence of the local uphill slopes on the up-dip flanks of the anticlines suggests that sedimentation has not completely kept pace with the structural growth.

Our quantitative results support the qualitative conclusions that workers have drawn from previous studies – namely that submarine channels seek out points of lowest relief and lowest relative uplift rate to make their way down slope (e.g., Huyghe et al., 2004; Ferry et al., 2005; Clark and Cartwright, 2009; Morley, 2009; Mayall et al., 2010 amongst others). In addition, we find that fault-propagation folds with very little positive bathymetric relief – associated with an uphill slope of no more than 2 km long (Fig. 16a, b); and whose contemporary interval strain rates are between -0.002 to -0.0022 $Ma^{-1}$ (-5 and $-7.2 \times 10^{-17}$ $s^{-1}$) can be incised by modern seabed channels that are active at the same time. However, for the detachment fold whose positive bathymetric relief is associated with a longer 5 km wavelength of uphill slope, even a comparatively lower maximum strain rates of -0.0023 $Ma^{-1}$ ($-7.3 \times 10^{-17}$ $s^{-1}$) can cause enough tilting of the seabed and force channels to be diverted around the tip of the fold. These results suggest that where channels have already developed, and are cutting through a growing structure, they are likely to be able to keep pace with growth rates on the order of 0.0022 $Ma^{-1}$ once the uphill slope length is not more than 2 km as seen in the fault-propagation folds. However, these channels could be diverted if the uphill slope was already in place) prior to channel development. Secondly, broad structures with longer wavelength of uphill slope will cause channels to divert (such as the diversion of Channel 2 by Fold C, Fig. 2a). But if the channel was already in place, it might be forced to abandon its original path, or migrate laterally as a response to continued seabed tilting as the structure widens through time.

We note that there are further factors that are likely to play an important role in channel incision through growing structures. These include both the erosive power and flow frequency of the sediment gravity flows within the channels. Channels with lower erosive power will be forced to divert and those with higher erosive power may be able to continue to incise and maintain a pathway through a growing structure (see also Morley, 2009; Mayall et al., 2010).

While variation in strain is useful in determining channel response to growing structures as demonstrated in this study, it is important to note that using displacement – distance plots to identify strain minima for prediction of sediment pathways can be misleading if these displacement measurements are not made for strata that actually bracket the time interval of channel system activity. We have demonstrated that fold growth rates have not been constant through time, and that areas with high cumulative displacement may nonetheless have accumulated relatively small amount of strain in the recent geological past. In a number of examples, positions of fold/thrust linkage remain persistent regions of low displacement during the life of fold growth (e.g., Fold B, Fig. 13). Yet for some folds (e.g., Folds A, C), the regions of low displacement may vary during the life of fold growth (*cf.* Fig. 13).

### 5.4 Implications for the structural evolution of the Niger Delta

#### *5.4.1 Strain rate reduction in last 3.7 Ma*

An important result of the study is that over the 40 km transect of the study area the four thrusts with seabed expression all show a reduction in shortening in the last 3.7 Ma, and that many of the buried thrusts between those studied, appear to have stopped moving within the lower part of the 3.7 Ma-Recent interval (Fig. 3). This reduction in growth during the later stages of fold growth may be due to the fact that (i) growth is now mainly being taken up by the younger thrusts/folds which have formed further basinward at the down-dip toe of the outer fold and thrust belt, or (ii) there has been an overall reduction in deformation rate on the entire Niger Delta gravitational system in the Plio-Pleistocene.

Although both explanations are plausible, recent work by Rouby et al. (2011) suggests that second reason given above for the slow-down in growth is the more likely. Using a detailed stratigraphic framework at high temporal resolution, they demonstrate a slow-down of both the amount and rate of deformation in the upslope extensional domain in the Plio-Pleistocene of the eastern Niger Delta in the last 4 Ma. Their work also shows that deformation slowed down in the compressional domain within the same time-frame, indicating a strong coupling between the deformation in the extensional and compressional domains, as is expected in a gravity-driven system. Our data are consistent with this interpretation. Rouby et al. (2011) attribute the slow-down in the extension to a decrease in sediment supply reaching the delta. The reduction in sedimentary load leads to a reduction in strain rate on the extensional faults, which then translates down-slope to lower rates of shortening. The reduction in sedimentary load is supported by the work of Jermannaud et al. (2010) who reported a general reduction in sediment supply to the Niger Delta during the Plio-Pleistocene which they suggest may have been in response to the aridification of the East Atlantic region. These interpretations are particularly interesting because they suggest that the magnitude and distribution of sediment supply to gravity-driven systems play a key role in driving the structural evolution of the fold and thrust belt in a potentially similar way to that suggested for terrestrial settings (e.g. Simpson, 2006).

*5.4.2 Sequence of thrusting*

A further observation that arises from our study, is that across the ~40 km wide transect through the outer fold and thrust belt there is no evidence for simple forward-propagating (or piggyback) thrusting as is often predicted for fold and thrust belts (Fig 3). Whilst the timing of onset of thrusting was not examined for all the structures in the study area, the four thrusts studied in detail all started to form at the same time, at least within the constraints of the available stratigraphic data. As these thrusts continue to grow, others in between have stopped moving within the last 3.7 Ma (Fig. 3).

Two sequentially restored structural sections through the inner and outer fold and thrust belts by Corredor et al. (2005), located very close to our study area, document that at a regional scale the inner fold and thrust belt started to form earlier than the outer fold and thrust belt and that the frontal thrust of the entire system is the youngest thrust. They also show that at a more local scale, such as that of our study area, a complex sequence of thrusting can be observed which can include forward- propagation (i.e. piggyback), backward propagation and coeval thrusting. Thus the observation of synchronous growth on the four structures studied for our work is consistent with the structural restoration results of Corredor et al. (2005).

Both analogue (e.g. Colletta et al., 1990; Huiqi et al, 1992; Storti et al. 1997) and numerical models of thrust belt development (Simpson, 2006, Stockmal et al., 2007) show that in the earliest phases of development of a fold and thrust belt the thrusts tend to develop by in-sequence, forward-propagation, with the youngest thrust forming in the most outboard position. As the belt continues to shorten older thrusts become inactive and are carried along passively (e.g. Colletta et al 1990), but in general overall forward propagation tends to dominate. However this is not what we, nor Corredor et al., observe for the Niger Delta and we would concur with the conclusion drawn by Corredor et al. (2005) that the sequence of thrusting in the deepwater Niger Delta does not obey the simple rules that are commonly used to prescribe the thrusting sequence in fold and thrust belts. However recent dynamic numerical models which incorporate syn-kinematic sedimentation appear to be able to replicate some of the observations from the Niger Delta. For example Stockmal et al. (2007), show that as the deformation progresses, older formed thrusts do not stop moving, and that deformation can localize behind the deformation front and focus on a few older thrusts, whilst others become inactive. Out-of-sequence thrusts are also common in some of these models particularly in the later phases of the model when the total amount of shortening increases. Although the Stockmal et al (2007) models were constructed to investigate tectonically driven fold belts, and hence incorporate, flexural loading, erosion as well as syn-kinematic sedimentation, its seems that some of their results may be applicable to the structures observed in deepwater passive margin fold belts where deformation is driven by gliding or spreading. This suggests that more sophisticated mechanical models incorporating a range of parameters that include varied strengths and rheologies for the basal décollement, pore-fluid pressure (important for settings such as the Niger Delta), multi-layer rheologies for the deforming strata, and sedimentation may assist us in understanding more fully the parameters that affect the kinematics of deepwater, gravity driven fold and thrust belts. It also leads to the intriguing suggestion that deepwater fold and thrust belts may have some similarities with their tectonic counterparts, where coupling and feedback between structural evolution and surface processes has been shown to be important (e.g. Willett, 1999; Simpson 2006; Stockmal et al. 2007)

## 6. Conclusions

• We have reconstructed temporal and spatial variations in cumulative strain and strain rates for the four thrusts-related folds that actively deform the modern seabed in the deep water Niger Delta. The maximum interval strain rate occurred between 9.5 Ma and 3.7 Ma, and has reduced significantly in the last 3.7 million years. This reduction in strain rate is attributed to the slow-down in gravity-driven deformation on the Niger Delta as a whole, in response to a reduction in sediment supply to the delta.

•The highest interval strain rates for the fault-propagation folds studied are between 0.02 and 0.06 $Ma^{-1}$ (equivalent to 1E-16 and -15 $s^{-1}$). The detachment fold, Fold C, has much lower maximum interval strain rate values (< -0.01 $Ma^{-1}$). The total shortening for the structures varies from 3810 m (Fold D) to 1072 m Fold (C) giving a time-averaged maximum shortening rate of between 350 $\pm$50 and 90 $\pm$10 m/Myr (0.4 and 0.1 mm/yr). Lower shortening rates of between 50 $\pm$5 and 40 $\pm$5 m/Myr (0.05 and 0.04 mm/yr) were recorded in the last 3.7 Ma when the channels studied were active.

• Submarine channels that developed coevally with structural growth cross the fault propagation folds in the central and western parts of the study area in positions of recent strain minima and at interval strain rates that are generally less than -0.02 $Ma^{-1}$ (i.e., -15 m per million years or ca. -1 x $10^{-16}$ $s^{-1}$) or at a cut-off rate of approximately -0.001 to -0.002 $Ma^{-1}$ (-5 to -7 x $10^{-17}$ $s^{-1}$). However the broad detachment fold (Fold C) has caused channel diversion of up to 25 km at an even lower strain rate of -0.002 $Ma^{-1}$ (-7 x $10^{-17}$ $s^{-1}$). We propose that this is due to the longer wavelength of the detachment fold which has a landward facing uphill slope of 1.5-2° extending laterally for up 5 km behind the fold crest, in comparison to similar magnitude slopes behind the fault propagation folds that only extend for 2 km. Additionally the ratio of sediment accumulation rate to the structural growth has most likely varied at temporal scales beneath the resolution of our biostratigraphic data. The stratal geometries suggest that there were periods in the last ca. 2 Ma when the growth rate of the detachment fold exceeded sediment accumulation leading to greater seabed bathymetric relief on this structure, during early phases of formation of the channel system, which most likely affected the channel pathway.

• Positions of low displacement may not be persistent in the same position of fold linkage during the life of the fold, and that implies shortening measurements using strata that bracket the time interval of the channel systems provide the best insights into the locus of channel-fold crossing points. This observation has important implications for the use of fold displacement – distance measurements in the prediction of sediment pathways through structures. Our results indicate that the use of cumulative displacement or shortening measurements are inappropriate for constraining the sensitivity of channel pathways to tectonic perturbation if they are made for strata that pre-date the existence of channel systems that cross the structure.

•Although our data gives new insights into the time-averaged interaction of fold-thrusts with submarine channels, an important avenue for future research is to consider how the episodic nature of both submarine channel incision/sedimentation and structural growth helps to control the timing and locus of channel diversion in tectonically active submarine settings.

## *Acknowledgements*

BAJ was funded by a Nigerian government Petroleum Technology Development Fund for his PhD. We thank Petroleum Geo-Services for providing the seismic data used for the research and for permission to publish seismic lines, and Shell Petroleum Development Company Nigeria for access to stratigraphic data. We acknowledge Halliburton Software and Services, a Halliburton Company, for providing the Landmark software used to interpret the seismic data under a university software grant. S. Gupta and H. Sinclair provided helpful advice on a first draft of the manuscript. Journal reviewers J. Bourget and I. Clark provided helpful comments.

**References**


Allmendinger, R., 1998. Inverse and forward numerical modeling of trishear fault propagation folds. Tectonics, 17, 640–656.

Anderson, J.E., Cartwright, J., Drysdall, S.J., Vivian, N., 2000. Controls on turbidite sand deposition during gravity-driven extension of a passive margin: examples from Miocene sediments in Block 4, Angola: Marine and Petroleum Geology, 17, 1165-1203.

Avbovbo, A.A., 1978. Tertiary lithostratigraphy of the Niger Delta. AAPG Bulletin, 62, 295-300.

Bernard, S.S., Avouac, J.-P., Dominguez, S., Simoes, M., 2007. Kinematics of fault-related folding derived from a sandbox experiment, Journal of Geophysical Research, 112, B03S12, doi:10.1029/2005JB004149.

Bergen K.J., Shaw, J.H., 2010. Displacement profiles and displacement-length scaling relationships of thrust faults constrained by seismic reflection data. GSA Bulletin 122, 1209-1219.

Bilotti, F.D., Shaw, J.H., 2005. Deep-water Niger Delta fold and thrust belt modelled as a critical-taper wedge: the influence of elevated basal fluid pressure on structural styles. AAPG Bulleting, 89, 1475-1491.

Briggs, S.E., Davies, R.J., Cartwright, J.A., Morgan, R., 2006. Multiple detachment levels and their control on fold styles in the compressional domain of the deep-water west Niger Delta. Basin Research, 18, 435–450.

Broucke, O., Temple, F., Rouby, D., Robin, C., Calassou, S., Nalpas, T., and Guillocheau, F., 2004, The role of deformation processes on the geometry of mud-dominated turbiditic systems, Oligocene and Lower-Middle Miocene of the Lower Congo basin (West African Margin): Marine and Petroleum Geology, v. 21, p. 327-348.

Burbank, D.W., Verges, N., 1994. Reconstruction of topography and related depositional systems during active thrusting. Journal of Geophysical Research, 99, 281-297.

Burbank, D., Meigs, A., Bronzovic, N., 1996. Interaction of growing folds and coeval depositional systems. Basin Research, 8, 199-223.

Burke, K.C.B., 1972. Longshore drift, submarine canyon, and submarine fans. AAPG Bulletin, 56, 1975-1983.

Cartwright, J. A., Trudgill, B.D., Mansfield, C. 1995. An explanation for the scatter in displacement and length data during fault growth by segment linkage. Journal of Structural Geology, 17, 672- 679.

Chapman, T.J., Williams, G.D., 1984. Displacement-distance methods in the analysis of fold-thrust structures and linked-fault systems. Geological Society London, 141, 121-128.

Clark, I. R., Cartwright, J. A., 2009. Interactions between submarine channel systems and deformation in deep-water fold belts: examples from the Levant Basin, Eastern Mediterranean sea. Marine and Petroleum Geology, 26, 1465-1482.

Clark, I. R., Cartwright, J. A., 2011. Key controls on submarine channel development in structurally active settings. Marine and Petroleum Geology, 28, 1333-1349.

Clark, I. R., Cartwright, J. A., 2012. Interactions between coeval sedimentation and deformation from the Niger Delta deep-water fold belt. SEPM Special Publication No. 99, 243–267.

Cohen, H.A., McClay, K., 1996. Sedimentation and shale tectonics of the northwestern Niger Delta front. Marine and Petroleum Geology 13, 313–328.

Colletta, B., Letouzey, J. Pinedo, R. 1990. Computerized X-ray tomorgraphy analysis of sandbox models: Examples of thin-skinned thrust systems. Geology, 19, 1063-1067.

Corredor, F., Shaw, J. H.  and Bilotti, F., 2005. Structural styles in the deep-water fold and thrust belts of the Niger Delta. AAPG Bulletin, 89, 753-780.

Cramez, C., Jackson, M.P.A., 2000. Superposed deformation straddling the continental-oceanic transition in deep-water Angola. Marine and Petroleum Geology, 17, 1095-1109.

Cronin, B.T., 1995. Structurally-controlled deep sea channel courses: examples from the Miocene of southeast Spain and in the Alboran Sea, southwest Mediterranean. In: Characterizationof Deep Marine Clastic Systems (Ed. by A.J. Hartley &D.J. Prosser). Geol. Soc. Lon. Sp Pub. 94; pp. 115–135

Daëron, M., Avouac, J.-P., Charreau, J., 2007. Modeling the shortening history of a fault tip fold using structural and geomorphic records of deformation, Journal of Geophysical Research, 112, B03S13, doi:10.1029/2006JB004460.

Dahlstrom, C.D.A., 1969. Balanced cross sections: Canadian Journal of Earth Sciences, 6, 743–757.

Damuth, J.E., 1994. Neogene gravity tectonics and depositional processes on the deep Niger Delta continental margin. Marine and Petroleum Geology, 11, 320–346.

Davis, K., Burbank, D.W., Fisher, D., Wallace, S., Nobes, D., 2005. Thrust-fault growth and segment linkage in the active Ostler fault zone, New Zealand. Journal of Structural Geology, 27 1528–1546.

De Sitter, L. V., 1956. Structural geology. New York, McGraw-Hill, 552 p.

Doust, H., Omatsola, E., 1990. Niger Delta, in: Edwards, J.D., Santogrossi, P.A.  (Eds.), Divergent /passive margin basins. AAPG Memoir, 48, 201-238.

Deptuck, M.E., Steffens, G.S., Barton, M., Pirmez, C., 2003. Architecture and evolution of upper fan channel-belts on the Niger Delta slope and in the Arabian Sea. Marine and Petroleum Geology, 20, 649-676.

Evamy, B.D., Haremboure, J., Kamerling, P., Knaap, W.A., Molloy, F.A., and Rowlands, P.H., 1978. Hydrocarbon habitat of Tertiary Niger Delta. AAPG Bulletin, 62, 277-298.

Fairhead, J.D., Binks, R.M., 1991. Differential opening of the Central and South Atlantic oceans and the opening of the West African rift system. Tectonophysics, 187, 191–203.

Ferry, J. N., Mulder, T., Parize, O., Raillard, S., 2005. Concept of equilibrium profile in deep water turbidite systems: effects of local physiographic changes on the nature of sedimentary processes and the geometries of deposits, in: Hodgson, D.M. and Flint, S.S. (Eds.), Submarine Slope Systems: Processes and Products. Geological Society London, 244, 181-193.

Ford, M., Williams, E.A., Artoni, A., Vergés, J., and Hardy, S., 1997, Progressive evolution of a fault-related fold pair from growth strata geometries, Sant Llorenç de Morunys, SE Pyrenees. J. Struct. Geol, 19, 413-441

Gawthorpe, R. L., Leeder, M. R., 2000. Tectono-sedimentary evolution of active extensional Basins. Basin Research, 12, 195 – 218.

Gee, M.J.R., Gawthorpe, R.L., 2006. Submarine channels controlled by salt tectonics: examples from 3D seismic data offshore Angola. Mar. Petrol. Geol., 23, 443–458.

Hardy, S., Poblet, J., 1994. Geometric and numerical model of progressive limb rotation in detachment folds. Geology, 22, 371–374.

Hardy, S., Poblet, J., 1995. The velocity description of deformation. Paper 2: sediment geometries associated with fault-bend and fault-propagaion folds. Marine Pet. Geol. 12, 165-176.

Hardy, S. Poblet, J. 2005. A method for relating fault geometry, slip rate and uplift data above fault-propagation folds. Basin Research, 17, 417-424.

Heinio, P., Davies, R.J., 2007. Knickpoint migration in submarine channels in response to fold growth, western Niger Delta. Marine and Petroleum Geology, 24, 434-449.

Heinio, P., Davies, R.J., 2006. Degradation of compressional fold belts: Deep-water Niger Delta. AAPG Bulletin, 90, 753–770.

Higgins, S., Davies, R.J., Clarke, B., 2007. Antithetic fault linkages in a deep water fold and thrust belt. Journal of Structural Geology, 29, 1900–1914.

Higgins, S., Clarke, B., Davies, R.J., Cartwright, J., 2009. Internal geometry and growth history of a thrust-related anticline in a deep-water fold belt. Journal of Structural Geology, 31, 1597–1611.

Hooper, R.J., Fitzsimmons, R.J., Neil, G., Vendeville, B.C., 2002. The role of deformation in controlling depositional patterns in the south-central Niger Delta, West Africa. Journal of Structural Geology, 24, 847-859.

Hossack, J.R., 1979. The use of balanced cross-sections in the calculation of orogenic contraction: A review. Geological Society London, 136, 705-711.

Huiqi, L., McClay, K., D Powell, D., 1992, Physical models of thrust wedges, in McClay (ed) Thrust Tectonics , Springer, 71-81.

Huyghe, P., Foata, M., Deville, E., Mascle, G., 2004. Channel profiles through the active thrust front of the southern Barbados prism. GSA Bulletin, 32, 429-432.

Jamison, W.R., 1987. Geometric analysis of fold development in overthrust terranes. J. Struct. Geol. 9, 207–219.

Jermannaud, P., Rouby, D., Robin, C., Nalpas, T., Guillocheau, F., Raillard, S. et al. 2010. Plio-Pleistocene sequence stratigraphic architecture of the eastern Niger Delta: A record of eustasy and aridification of Africa. Mar. Pet. Geol. 27, 810–821.

Knox, G.J., Omatsola, E.M., 1989. Development of the Cenozoic Niger Delta in terms of the 'escalator regression' model and impact on hydrocarbon distribution, in: Van Der Linden, W.J.M., Cloetingh, S.A.P.L., Kaasscheiter, J.P.K., Van Ger Graaf, W.J.E., Vandenberglie, J., Van Der Gun, J.A.M. (Eds.), Proceedings of the KNGMG Symposium Coastal Lowlands. Geology and Geotechnology, 181-202.

Li, T., Chen, J., Thompson, J.A., Burbank, D.W., Yang, X., 2013. Quantification of three-dimensional folding using fluvial terraces: A case study from the Mushi anticline, northern margin of the Chinese Pamir. Journal of Geophysical Research, 118, 4628 – 4647.

Maloney, D., Davies, R., Imber, J., Higgins, S., King, S., 2010. New insights into deformation mechanisms in the gravitationally driven Niger Delta deep-water fold and thrust belt. AAPG Bulletin, 94, 1401-1424.

Mascle, J., Marhino, M., Wanesson, J., 1986. The structure of the Guinean continental margin: implications for the connections between the Central and South Atlantic Oceans. Geologische Rundschau, 75, 57-70.

Mayall, M., Lonergan, L., Bowman, A., James, S., Mills, K., Primmer, T., Pope, D., Rogers, L., Skeene, R., 2010. The response of turbidite slope channels to growth-induced seabed topography. AAPG Bulletin, 94, 1011-1030.

Mitchum, R.M., Wach, G.D., 2002. Niger Delta Pleistocene levee-channel fans: models for offshore reservoirs. 22nd Annual Gulf Coast SEPM Foundation Bob F. Perkins Research Conference, 712-726.

Moretti, I, Callot, JP 2012. Area length and thickness conservation: Dogma or reality? J SG 41, 64-75

Morgan, R., 2004, Structural controls on the positioning of submarine channels on the lower slopes of the Niger Delta, in: Davies, R.J., Cartwright, J.A., Stewart, S.A., Lappin, M., and Underhill, J.R. (Eds.), 3D seismic technology: application to the exploration of sedimentary basins. Geological Society London Memoirs, 29, 45-51.

Morley, C.K., Guerin, G., 1996. Comparison of gravity-driven deformation styles and behaviour associated with mobile shales and salt. Tectonics, 15, 1154–1170.

Morley, C.K., 2009. Growth of folds in a deep-water setting. Geosphere, 5, 59-89.

Morley, C.K., Leong, L.C., 2008. Evolution of deep-water syn-kinematic sedimentation in a piggy-back basin, determined from 3d seismic reflection. Geosphere, April 2009, 89 data: Geosphere, 4, 938-962.

Normark, N. R., 1978. Fan valleys, channels, and depositional lobes on modern submarine fans: characters for recognition of sandy turbidite environments. AAPG Bulletin, 62, 912–931.

Oluboyo, A.P. Gawthorpe. RL. Bakke, K., Hadler-Jacobsen, F. 2014. Salt tectonic controls on deep-water turbidite depositional systems: Miocene, southwestern Lower Congo Basin, offshore Angola. Basin Research, 26, 597-620.

Poblet, J., and Hardy, S., 1995. Reverse modelling of detachment folds; application to the Pico del Aguila anticline in the South Central Pyrenees (Spain). Journal of Structural Geology, 17, 1707–1724.

Poblet, J., McClay, K., Storti, F., Muñoz, J.A. 1997. Geometries of syntectonic sediments associated with single-layer detachment folds. J. Struct. Geol. 19, 369-381.

Poblet, J., Bulnes, M., McClay, K., Hardy, S., 2004. Plots of crestal structural relief and fold area versus shortening—A graphical technique to unravel the kinematics of thrust-related folds, in:

Rowan, M.G., Peel, F.J., Vendeville, B.C., 2004. Gravity-driven fold belts on passive margins, in: McClay, K.R. (Ed.), Thrust tectonics and hydrocarbon systems: AAPG Memoir, 82, 157-182.

Rouby, D., Nalpas,T. Jermannaud, P., Robin, C., Guillocheau, F., Raillard, S. 2011. Gravity driven deformation controlled by the migration of the delta front: The Plio-Pleistocene of the Eastern Niger Delta. Tectonophysics, 513, 54-67.

Shaw, J. H., Novoa, E., Connors, C.D., 2004. Structural controls on growth stratigraphy in contractional fault-related folds, in: McClay, K.R. (Ed.), Thrust tectonics and hydrocarbon systems: AAPG Memoir, 82, 400 - 412.

Shaw, J.H., Connors, C.D., and Suppe, J., 2005, Seismic interpretation of contractional fault-related folds: An AAPG seismic atlas, AAPG Studies in Geology.

Short, K.C., Stauble, A.J., 1965. Outline of geology of Niger Delta. AAPG Bulletin, 51, 761-779

Simoes, M., Avouac, J.P., Chen, Y.-G., Singhvi, A.K., Wang, C.-Y., Jaiswal, M., Chan, Y.-C., Bernard, S., 2007. Kinematic analysis of the Pakuashan fault tip fold, west central Taiwan: Shortening rate and age of folding inception. Journal oF Geophysical Research, 112, B03S14, doi:10.1029/2005JB004198.

Simpson, G.D.H. 2006. Modelling interactions between fold-thrust belt deformation, foreland flexure and surface mass transport. Basin Research, 18, 125-143.

Stockmal, G.S. Beaumont, C., Nguyen, M., Lee. B. 2007. Mechanics of thin-skinned thrust-and-fold Belts: Insights from numerical models. In: Whence the Mountains? Inquiries into the Evolution of Orogenic Systems: A Volume in Honor of Raymond A. Price, Geological Society of America, editors J. Sears, T. Harms, and C. A. Evenchick, Spec. Paper 433, 63-99.

Storti, F., Poblet, J., 1997. Growth stratal architectures associated with décollement folds and fault propagation folds. Inferences on fold kinematics. Tectonophysics, 282, 353–373.

Storti, F., Salvini, F., McClay, K. 1997. Fault-related folding in sandbox analogue models of thrust wedges. J. Struct. Geol. 19, 583-602.

Suppe, J., Medwedeff, D.A., 1990. Geometry and kinematics of fault-propagation folding. Eclogae Geologicae Elvetiae, 83, 409–454.

Suppe, J., Chou, G.T., Hook, S.C., 1992. Rates of folding and faulting determined from growth strata. In: McClay, K.R. (Ed.), Thrust Tectonics. Chapman and Hall, London, 105–121p.

Walker, R. G., 1978. Deep-water sandstone facies and ancient submarine fans: models for exploration for stratigraphic traps. AAPG Bulletin, 62, 932–966.

Whiteman, A.J., 1982. Nigeria: its Petroleum Geology, Resources and Potential. Graham and Trotman, 1, 166p.

Willett, S.D. 1999. Orogeny and orography: the effects of erosion on the structure of mountain belts. J. Geophys. Res., 104, 28957-28981.

Wu, S., Bally, A. W., 2000. Slope tectonics-Comparisons and contrasts of structural styles of salt and shale tectonics of the northern Gulf of Mexico with shale tectonics of offshore Nigeria, in: Mohriak, W., Talwani, M. (Eds.), Atlantic rifts and continental margins. Washington, D.C., American Geophysical Union, 151-172.

| Fold | Uplift (m) | Uplift rate (m/Myr) | Shortening (m) | Shortening rate (m/Myr) | strain | Strain rate (Ma/Ma) | Strain rate ($s^{-1}$) |
|---|---|---|---|---|---|---|---|
| **A** | 218 | 59 | -216 | -58 | -0.0266 | -0.00719 | 2.3E-16 |
| **B** | 202 | 54 | -198 | -54 | -0.0265 | -0.00716 | 2.3E-16 |
| **D** | 216 | 58 | -204 | -55 | -0.0298 | -0.00805 | 2.6E-16 |
| **C** | - | - | -169 | -46 | -0.0107 | -0.00289 | 9.2E-17 |

**Table 1.** Values of maximum uplift, uplift rate, maximum shortening, shortening rate, maximum strain and strain rate since 3.7 Ma for the structurally highest fold crest of the fault-propagation folds (A, B and C) and the detachment fold (Fold C). See text for discussion of how the uplift and uplift rate are calculated.

**Figure captions**

Figure 1: (a) Bathymetry map of the Niger Delta (modified from Corredor et al., 2005) showing the structural zones of the Niger Delta and the study area. (b) Regional section across the Niger Delta (modified from Corredor et al., 2005) showing the structural styles from extension on the shelf to shortening in the toe-thrust area in the deep-water parts of the delta.

Figure 2: (a) 3D bathymetry map and (b) edge-attribute map of the seabed in the study area. The maps show modern, seabed channel systems (1, 2, 3 and 4) and growing folds with seabed relief (A, B, C and D). The trace of the fold axes at the seabed is shown as sold lines with diamonds; the dashed fold axes are folds that do not have bathymetric expression at the modern sea floor. (c) Map of main thrusts and folds present at approximately 550 ms Twtt beneath the seabed. Folds with seabed relief are in brown, and the associated thrusts in red. Section lines, a1, a2, a3, b1, b2, c1, c2 and d1, d2 across folds are shown in Figures 8, 9, 10, and 16. Black to white gradient on edge-attribute map is high to low slope dip.

Figure 3: (a) Uninterpreted and (b) interpreted seismic cross-section across the study area illustrating the general structural style (See Fig. 2b for location). The structures consist of fore-thrusts that detach within the Akata Formation shales, and back-thrusts that mostly intersect the fore-thrusts. Syn-growth units can be identified by stratal thickness changes towards fold crests and in inter-thrust synclines.

Figure 4:Isochron map of the growth sequence interval over the study area showing a series of NW – SE orientated depocentres (blue areas) and growing folds (yellow areas). The depocentres correspond to the footwall and hanging wall synclines of the actively growing structures. Labelled folds are those studied in detail.

Figure 5: Methodology used for measuring strain based on line-length balancing. $L_f$ = the present day length of the section while the original bed length is defined as $L_0$ . $L_0$ for pre-growth horizons = $P_1$ + $P_2$ and $L_0$ for syn-growth strata = S.

Figure 6: Seismic sections across Folds A and Fold B, illustrating potential seismic interpretation problems and how they are treated. Section a, shows a palaeo-scarp and the interpretation in b, shows the extrapolation of horizon h3 across the palaeo-scarp in order to measure strain. Section c, shows a seabed scarp and the interpretation in d, shows how the scarp is smoothed in order to measure strain on the seabed. Section e, shows channel incision across growing folds and the interpretation, f, shows extrapolation of horizon h3 across the erosive base of the channel in order to measure strain.

Figure 7: (a) Seismic section across Fold A (section a2; Fig. 2a); stratigraphic horizons used for strain measurements are labelled. (b) Plot of cumulative strain for two different depth conversion seismic velocities of 2300 and 2500 m/s; (c) interval strain rates derived from (b).

Figure 8: Uninterpreted (a, c) and interpreted (b, d) seismic sections across Fold A (See Figure 2a for location). These sections reveal the structural style of the fold with a fore-thrust that detached within the Akata shales, and a back-thrust that intersects the fore-thrust.

Figure 9: Uninterpreted (a, c, e) and interpreted (b, d, f) seismic sections across Folds B and D; (sections located in Figure 2a). These sections all show composite thrust-related folds each with two fore-thrusts. Note that only one of the folds has a significant influence on the seabed and the other is buried. Note also that there is a palaeo-scarp in (a, b); and the folds in (c, d) have been cut by an active seabed channel.

Figure 10: Uninterpreted (a) and interpreted (b) versions of section c1 across Fold C (located in Figure 2a). Fold C has low displacement planar thrusts in its front and back limbs, and is cored by a duplex within the Akata shales.

Figure 11:(a) and (b) seismic section across a buried channel and channel 4 illustrating how the downlap surface of channels levees is used as a proxy to estimate channel age. (c) Sea-bed edge map illustrating channel-structure interaction.

Figure 12: (a) Graph of cumulative strain against stratigraphic age for sections a1, b1, c2 and d1 (located on Figure 2a). (b) Interval strain rate plotted against stratigraphic age (i.e., the gradient of curves shown in (a)). These plots show variations in the interval strain rate through time. The maximum interval strain rate for all folds occurred between 9.5 Ma and 3.7 Ma; and all folds show a significant reduction in interval strain rate in the last 3.7 million years.

Figure 13: Graph of cumulative strain versus distance along strike for folds A to D. The blue curve is the strain for 23.2 Ma, red for 7.4 Ma and green for the 3.7 Ma horizons respectively. The present day seabed relief is shown in purple. The strain decreases as the horizons become younger, reflecting the growth of the structures through time.

Figure 14: (D1) Cumulative strain of stratigraphic horizons in Fold D; (D2) seabed map showing the outline of Fold D and relative position of Channel 4; (D3) interval strain rates measured at locations [1] and [2] shown in D1, and represented by the black and brown bars respectively. (A1) Cumulative strain of stratigraphic horizons in Fold A;(A2) seabed map showing the outline of Fold A and relative positions of seabed channels; (A3) interval strain rates measured at location [1] shown in A1. (B1) Cumulative strain of stratigraphic horizons in Fold B; (B2) seabed map showing the outline of the composite Fold B and relative position of seabed channels, (B3) interval strain rates measured at locations [1] shown in B1. (C1) Cumulative strain of stratigraphic horizons in Fold C, (C2) seabed map showing the outline of Fold C and relative position of Channel 2, (C3) interval strain rates measured at location [1] shown in C1. Distances on x-axes are measured from NW end of structures.

Figure 15: Simple diagrams to illustrate end-member relationships between structural uplift rate and sediment accumulation rate. (a) Higher sediment accumulation rate relative to uplift rate where the syn-growth sediments (pink) overlap the growing structure. Because of lack of bathymetric relief associated with the growing fold seabed channels can cross over the fold crest as shown schematically in (b). (c) Higher uplift rate relative to sediment accumulation rate with the syn-growth sediments (pink) onlapping the growing structure. This scenario generates seabed relief and any channels crossing the area are likely to be deflected away from the fold-related seabed relief as shown in (d).

Figure 16: (a) Section across Fold A (section a3 in Figure 2a) showing mainly overlapping seismic horizons over the structure since 3.7 Ma (although these horizons have been truncated by the

seabed scarp); this indicates a slightly lower uplift rate relative to sedimentation rate. Note that the uphill slope is 1.8 km in length. (b) Section across Fold D (section d2 in Figure 2a) also showing the same geometric relationship as in (a). Note also that the uphill slope is ~ 2 km in length and the overlapping horizons have been truncated by a scarp. (c) Section across Fold C (section c2 in Figure 2a) showing seismic horizons which largely onlap the growing structure since 3.7 Ma – although there are periods of minor offlap (continuous yellow lines) which indicate variation in growth rate through time. The overall onlapping geometry indicates a slightly higher uplift rate relative to sedimentation rate. Note that the uphill slope is ~ 5.6 km in lateral extent.

Table 1: Values of maximum uplift, uplift rate, maximum shortening , shortening rate, maximum strain and strain rate since 3.7 Ma for the structurally highest fold crest of the fault-propagation folds (A, B and C) and the detachment fold (Fold C). See text for discussion of how the uplift and uplift rate are calculated.

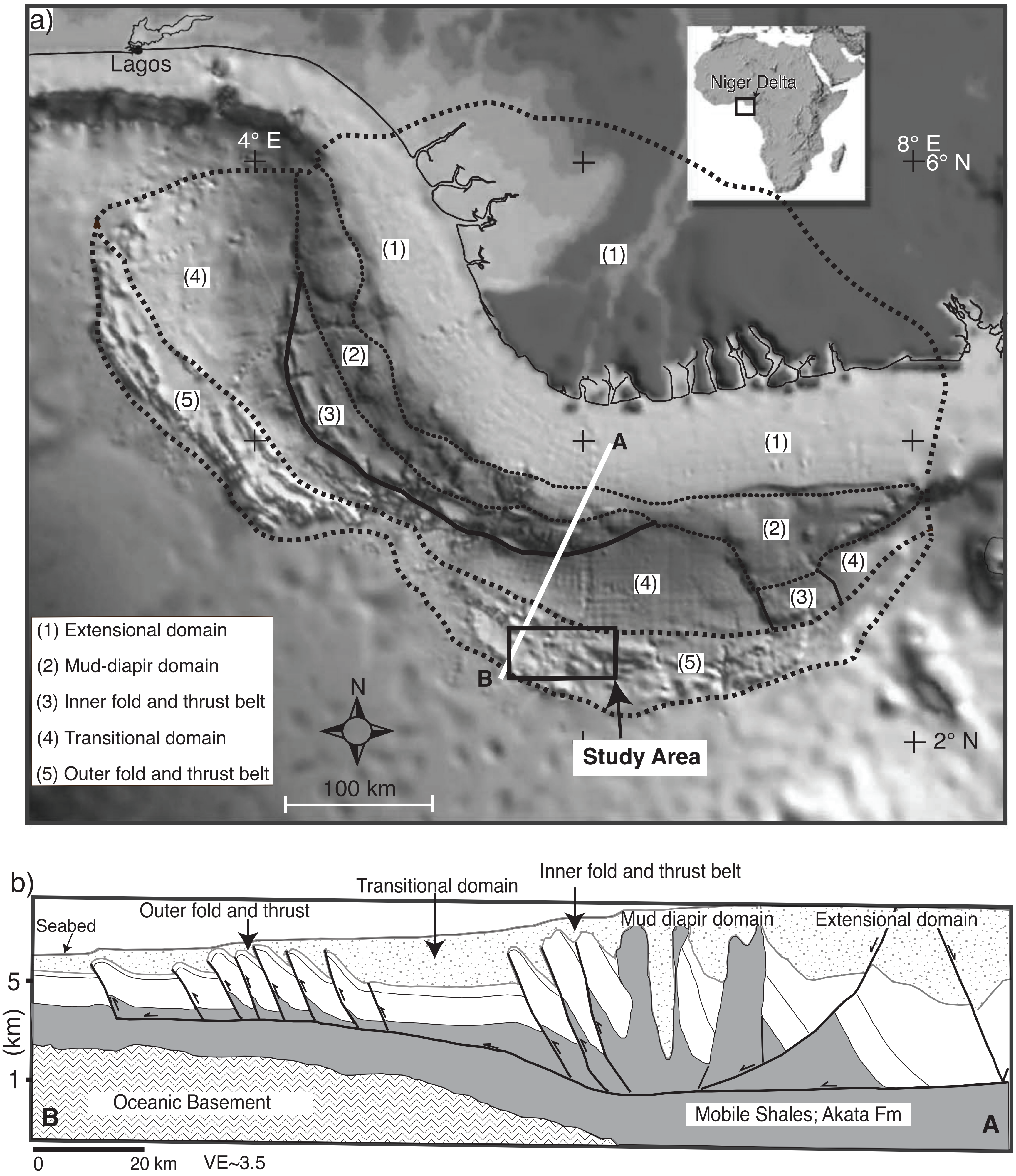


Figure 1 Jolly et al

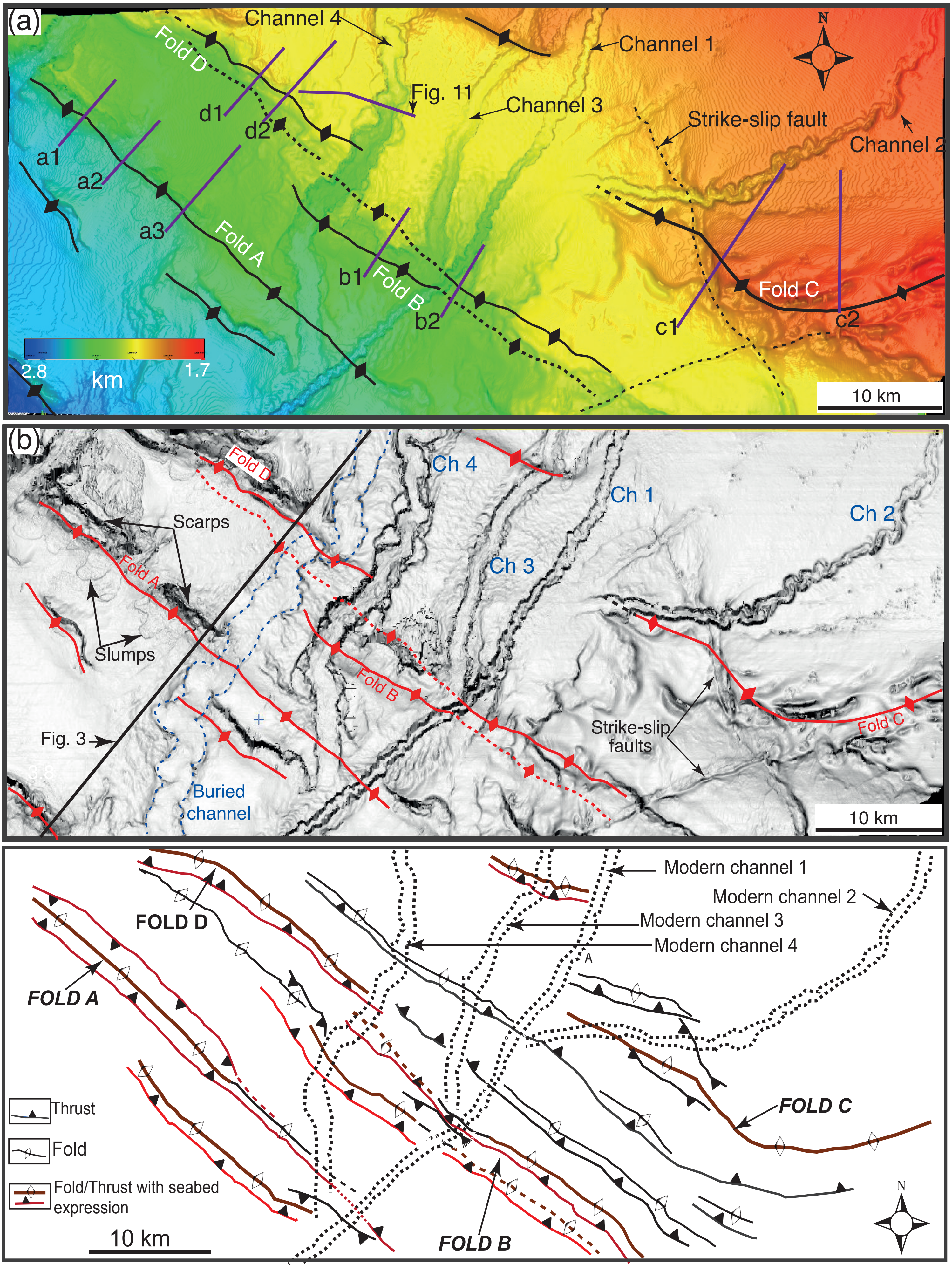


Figure 2 Jolly et al.

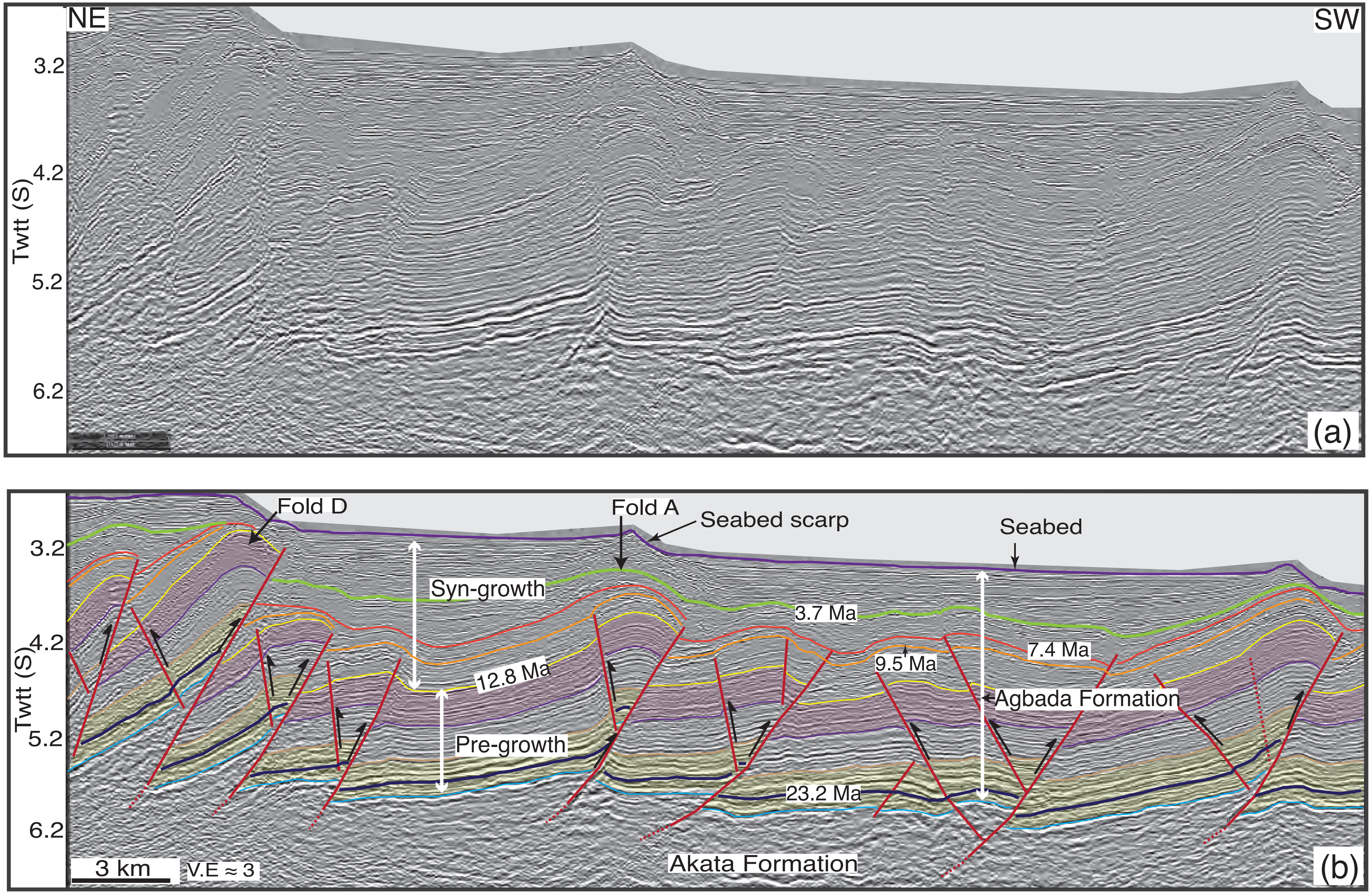


Figure 3; Jolly et al.

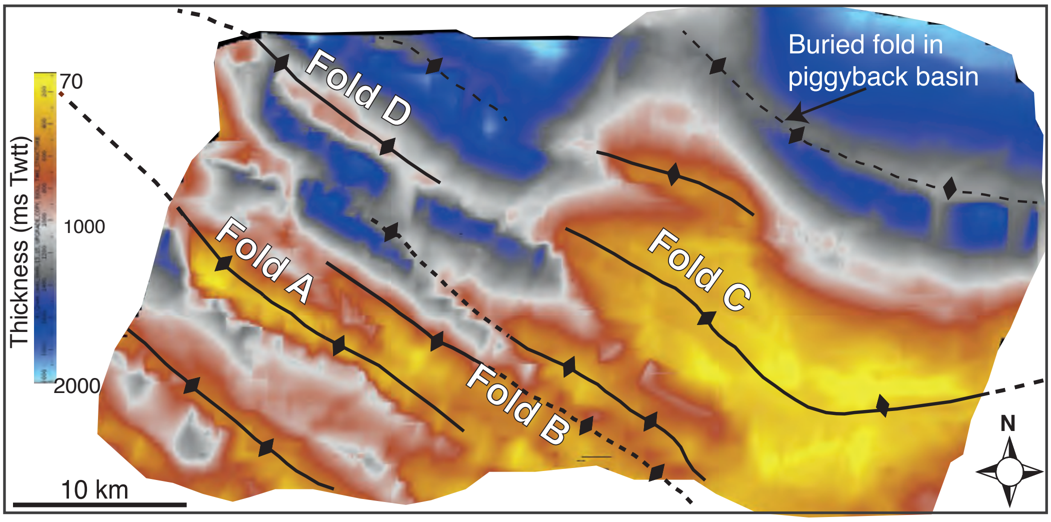


Figure 4; Jolly et al.

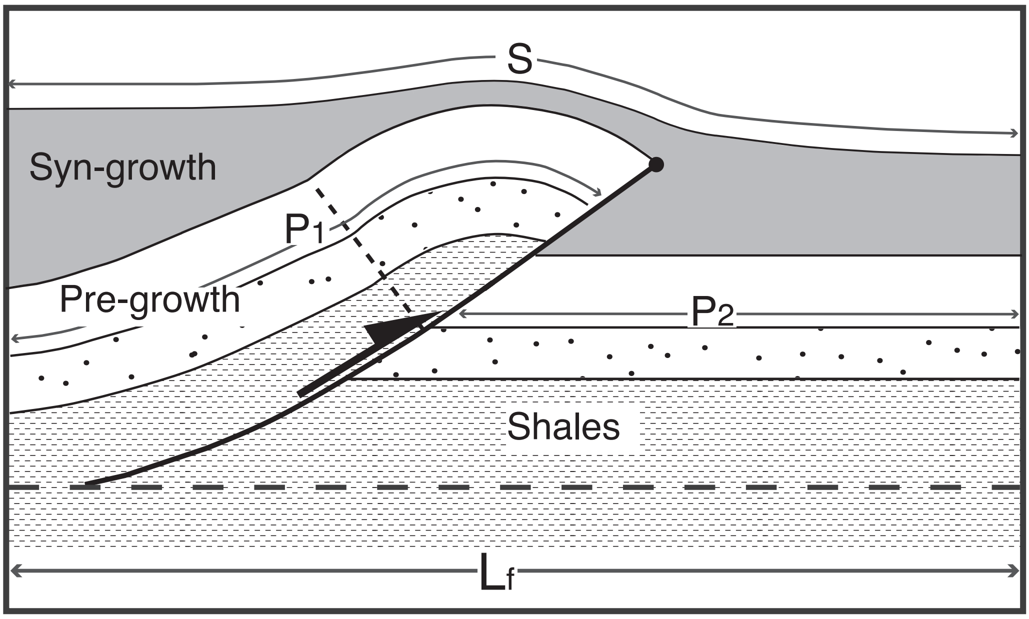


Figure 5. Jolly et al.

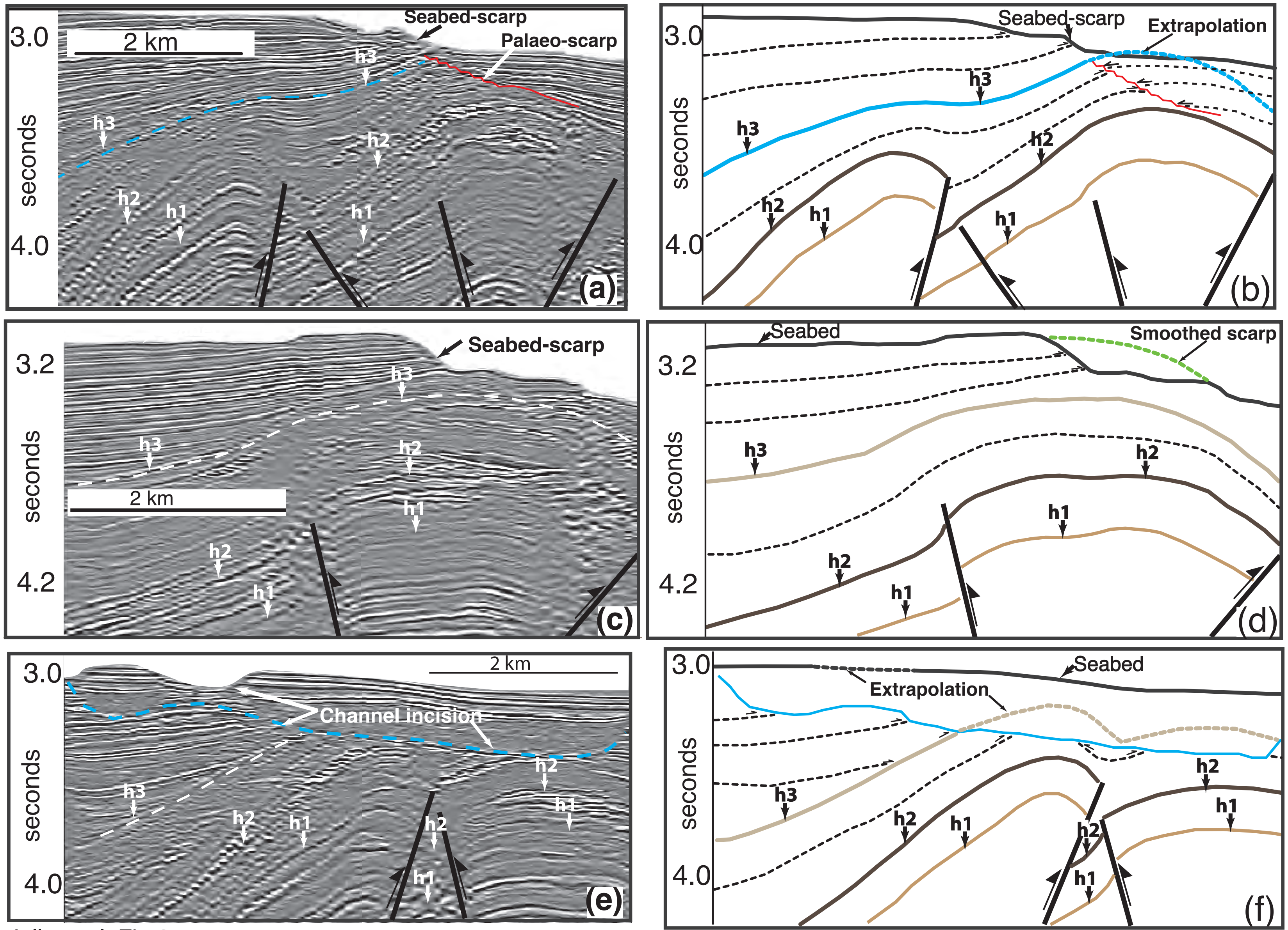


Jolly et al. Fig 6

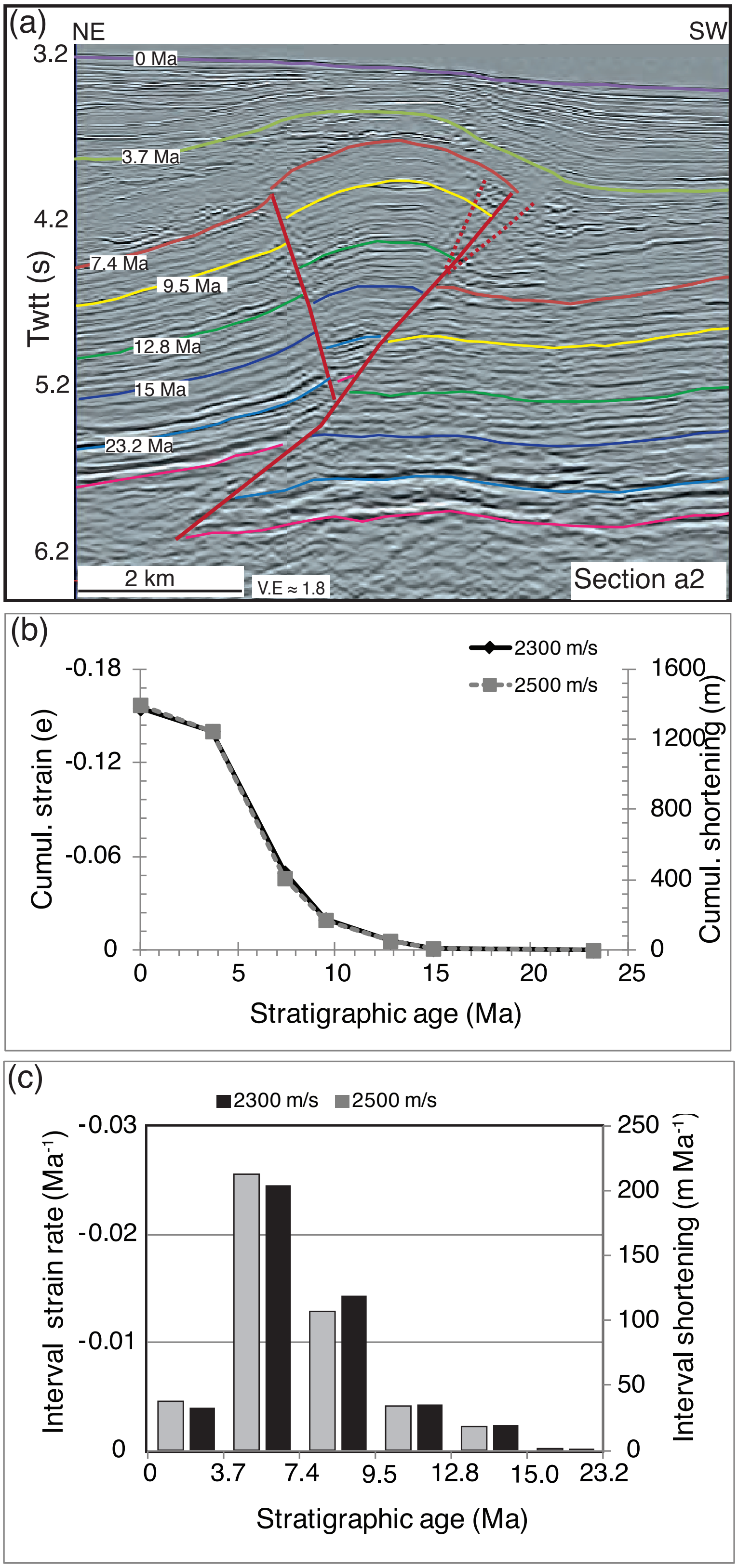


Figure 7; Jolly et al.

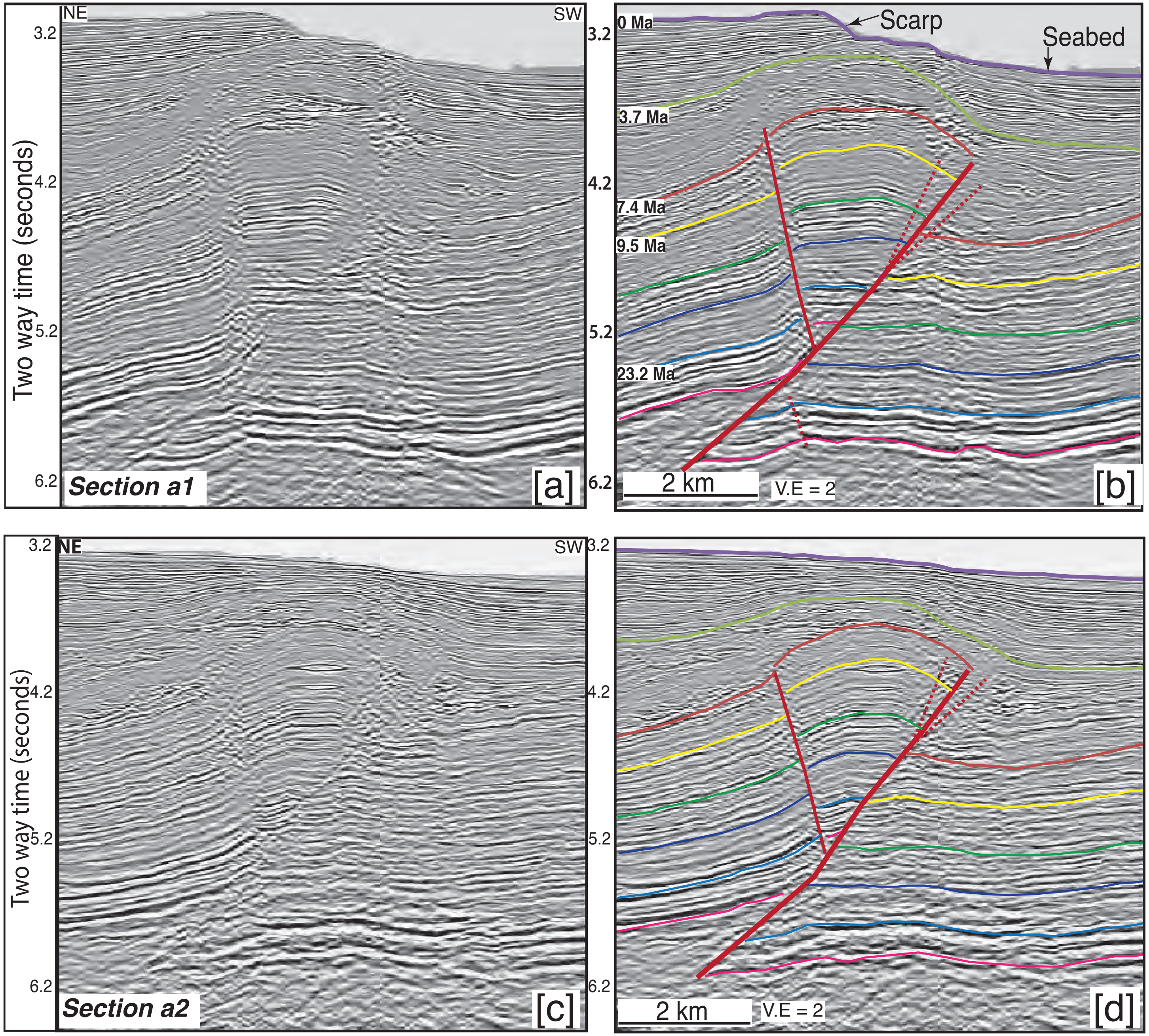


Figure 8 Jolly et al.

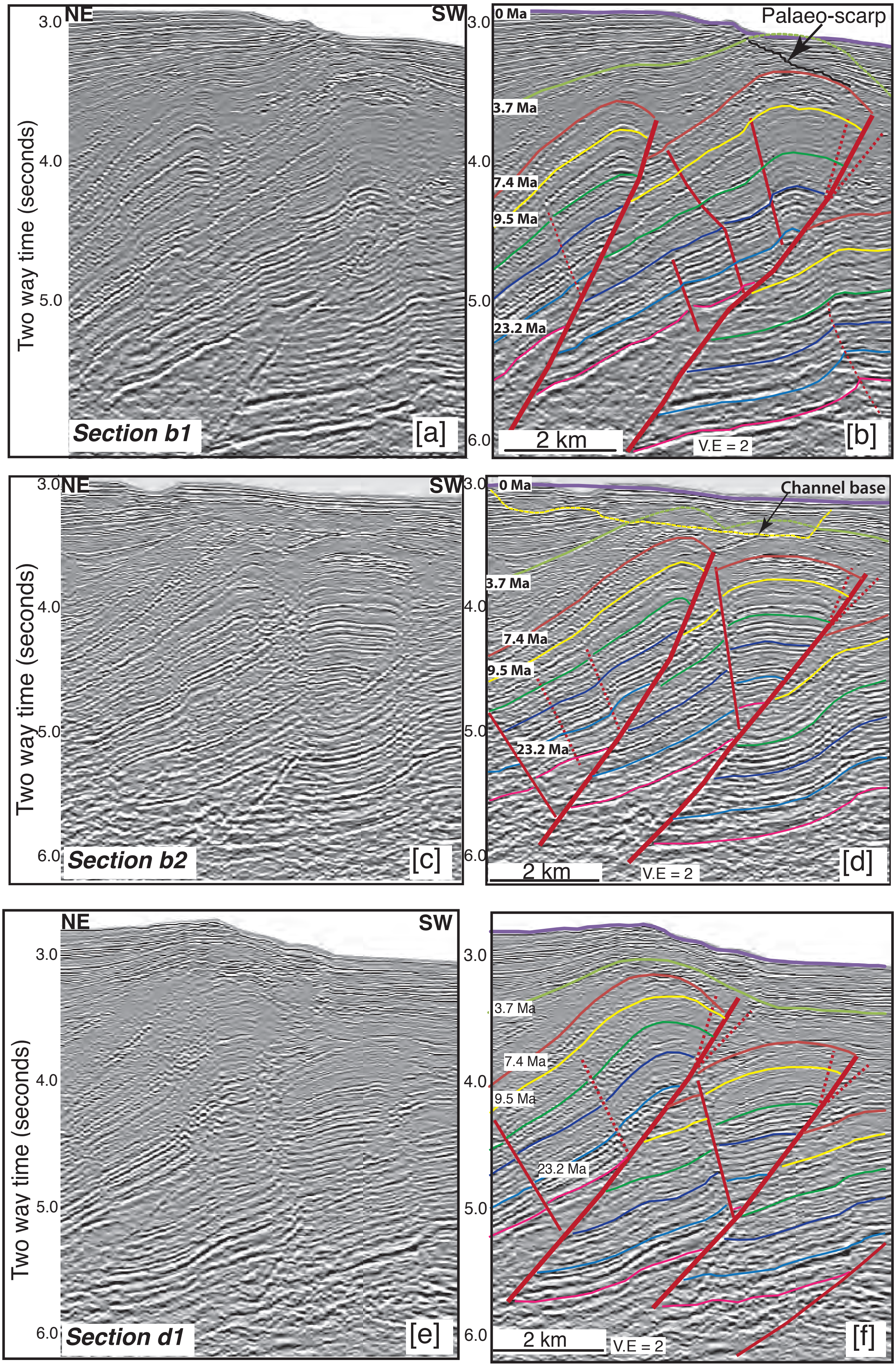


Jolly et al. Fig 9

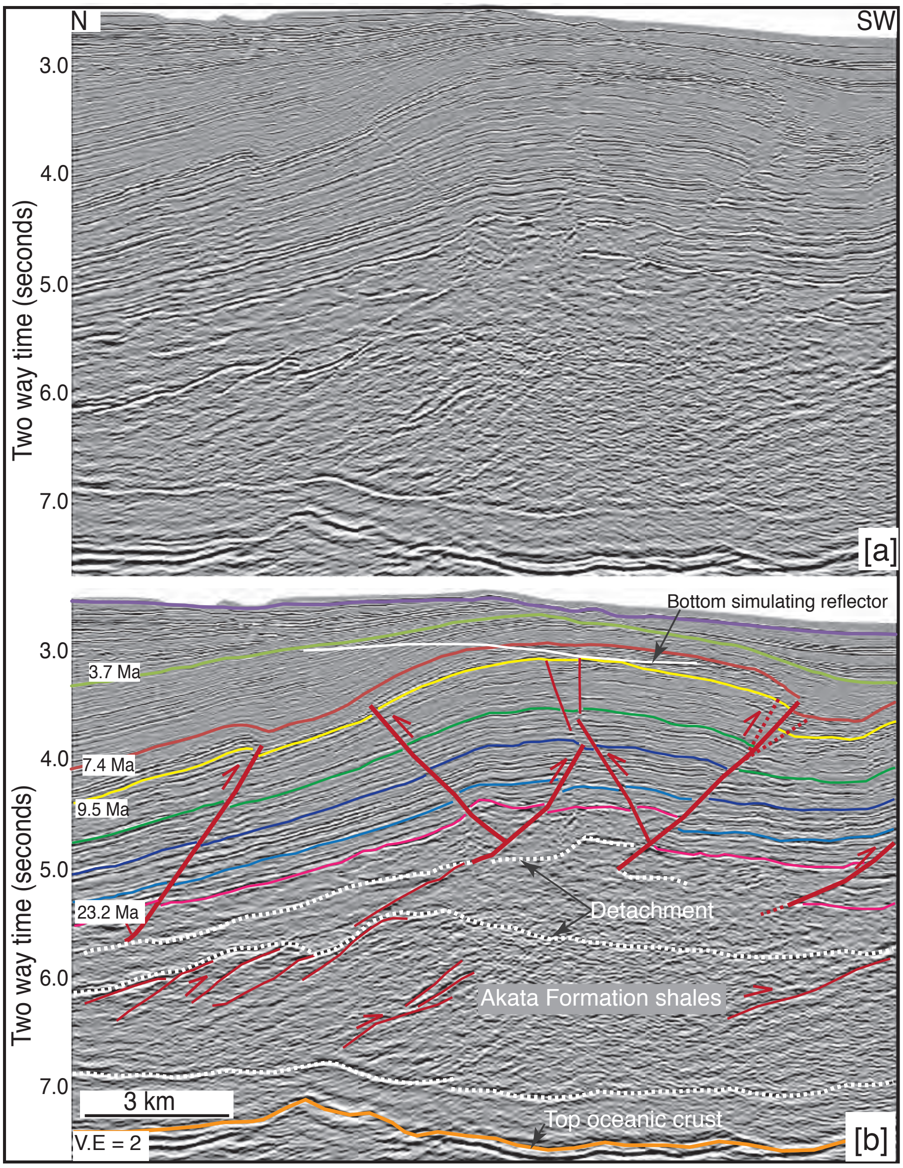


Jolly et al. Figure 10

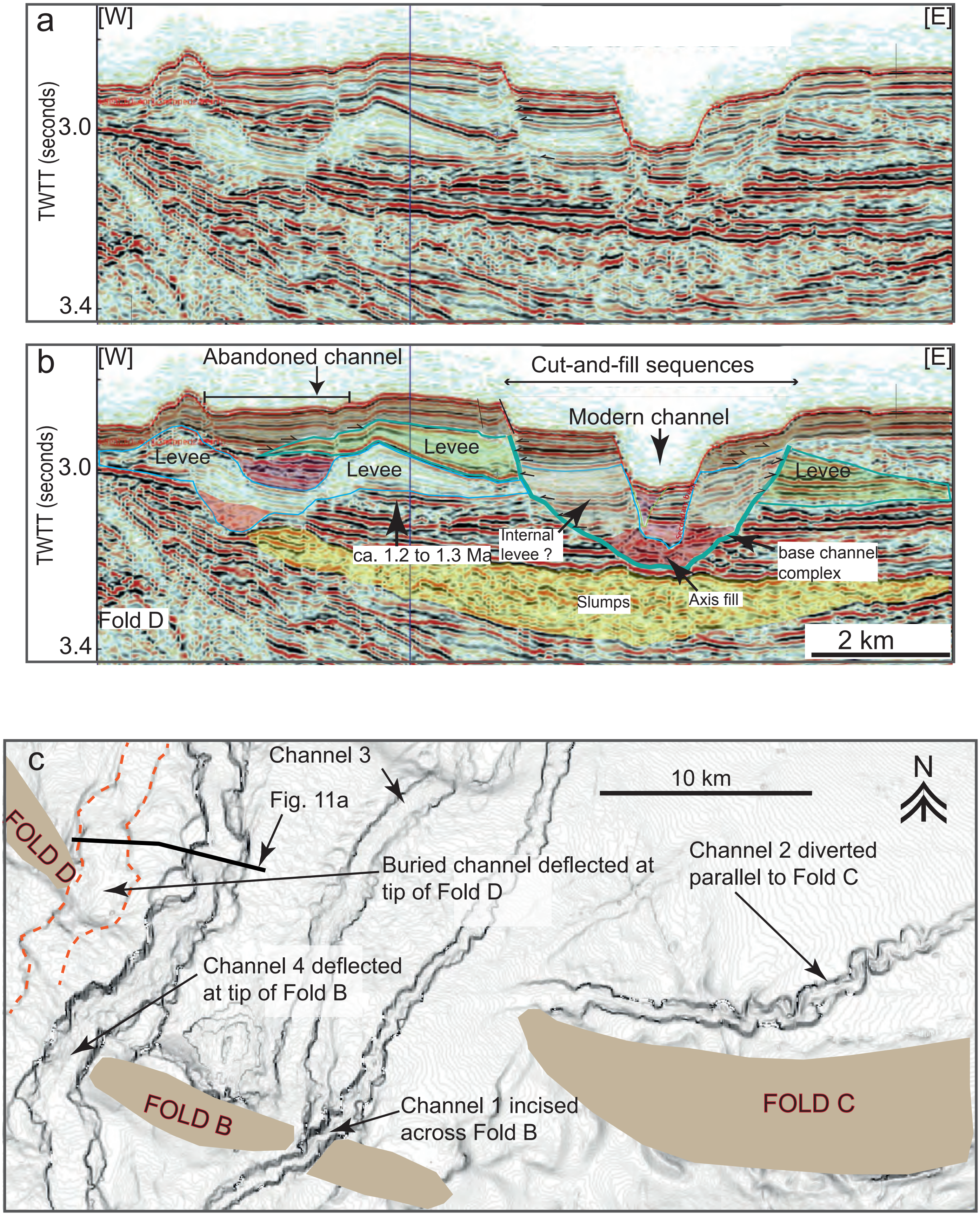


Figure 11; Jolly et al.

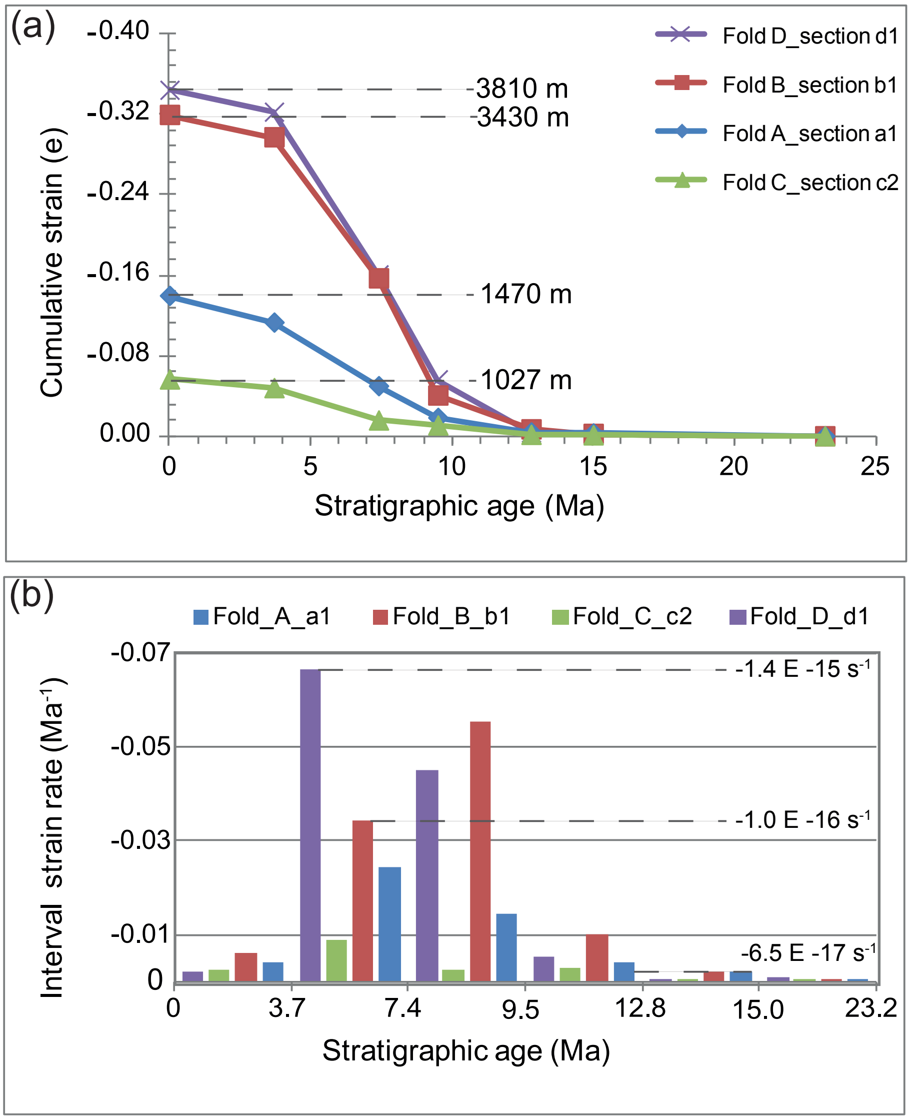


Jolly et al fig 12

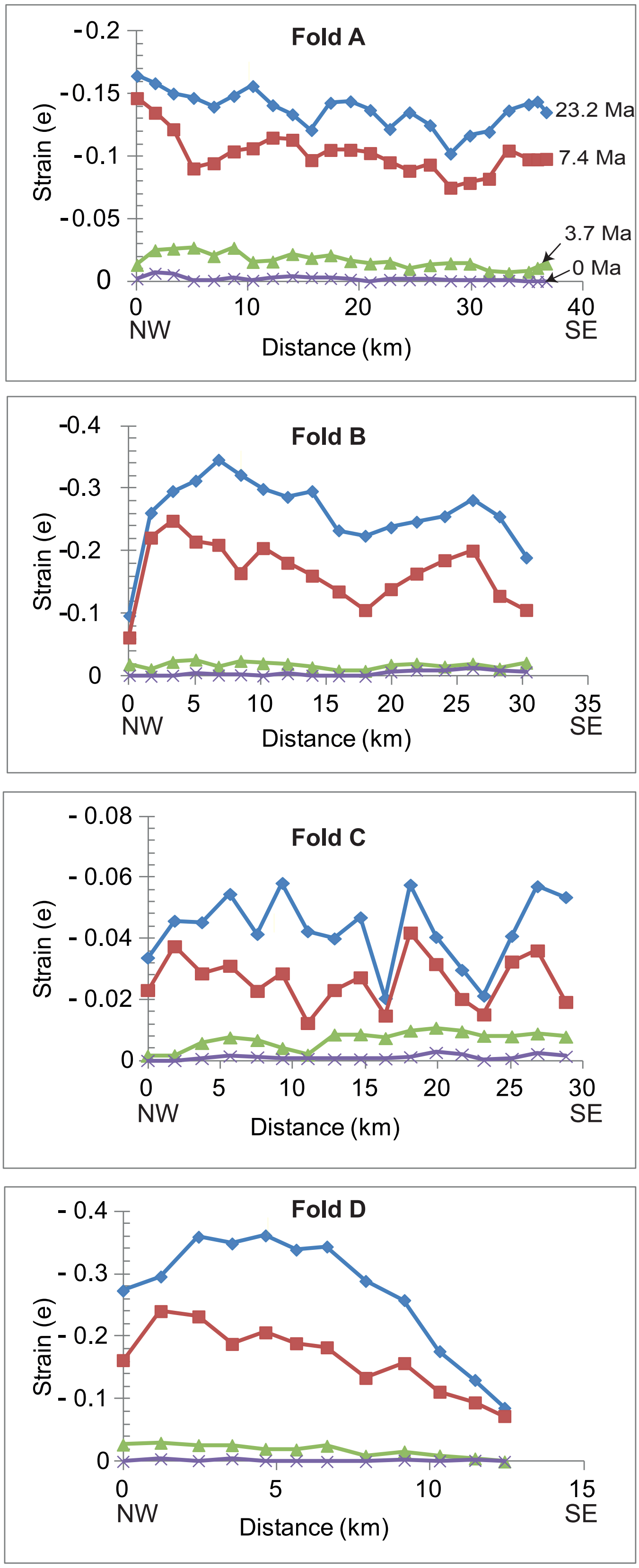


Jolly et al fig 13

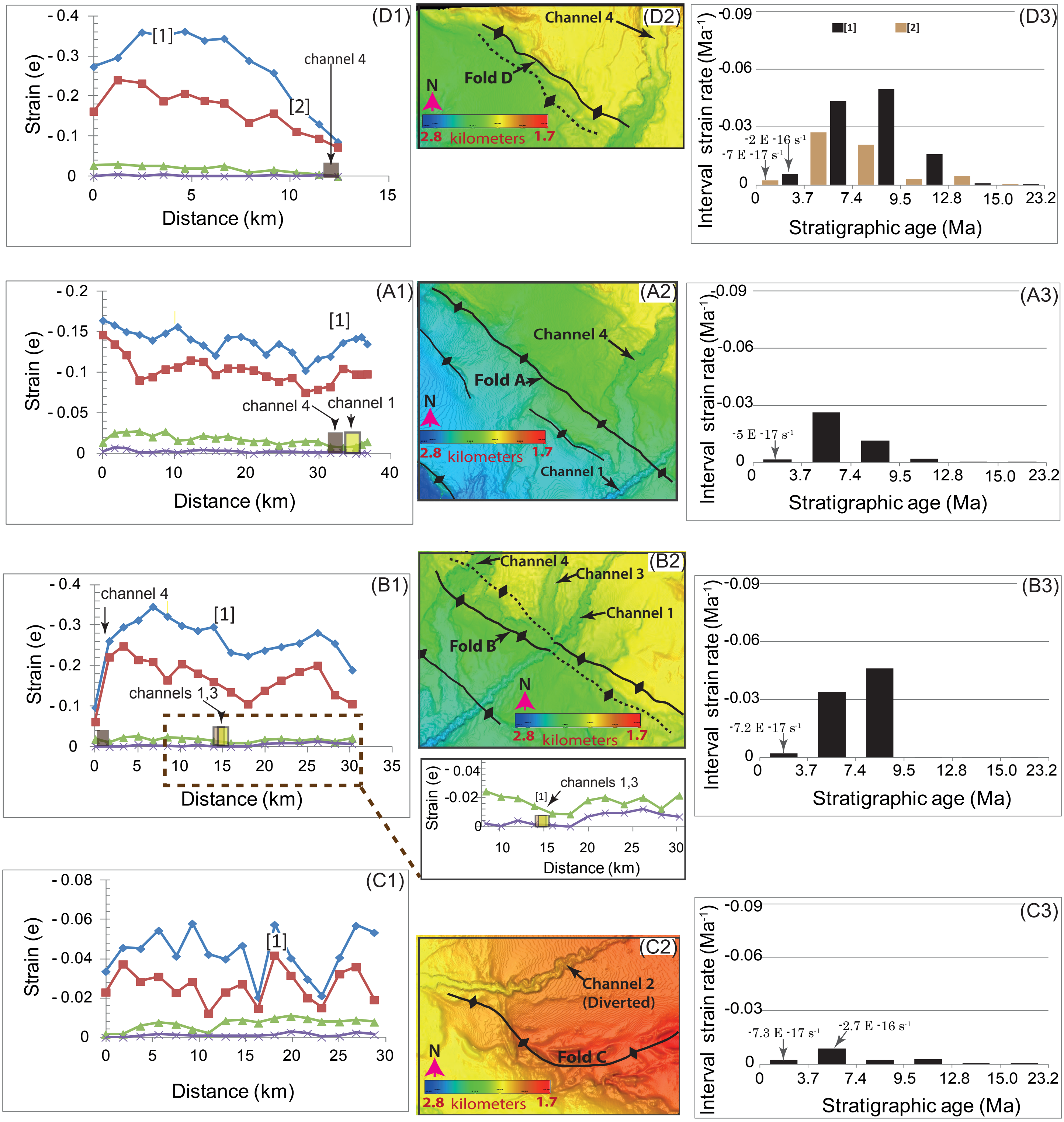


Jolly et al fig 14

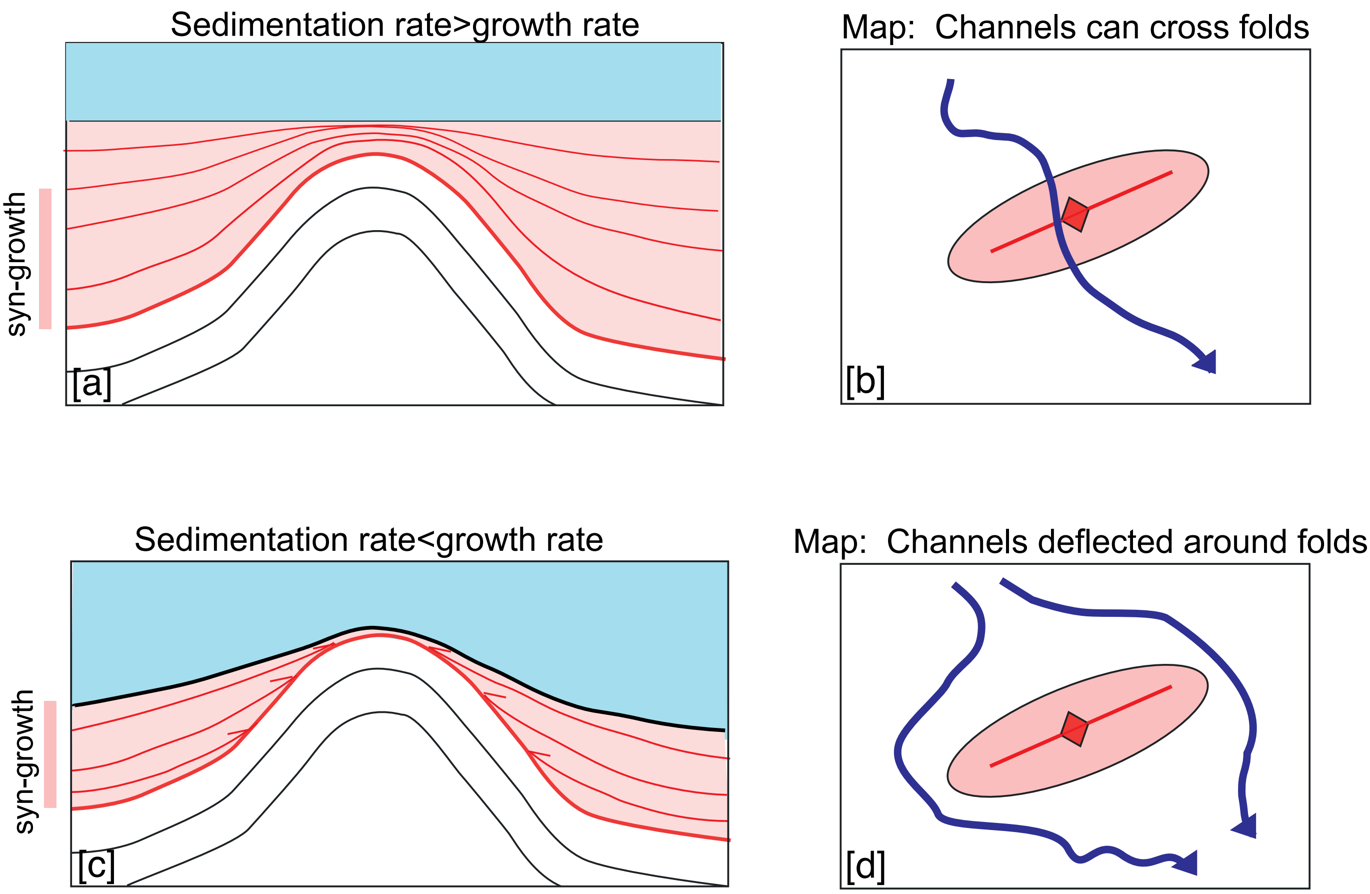


Jolly et al. Fig 15

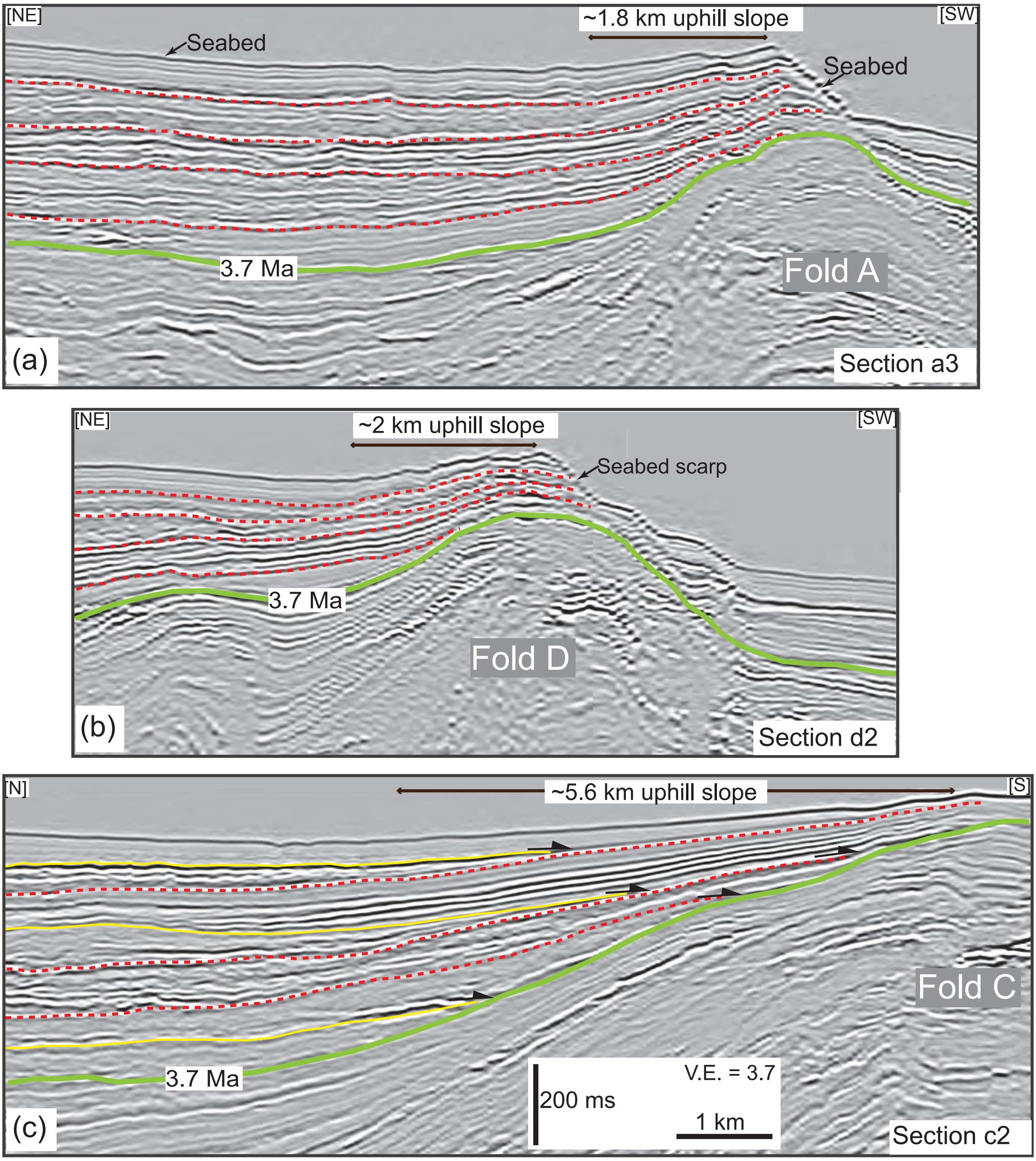


Figure 16 Jolly et al.